

AGB Mapping using Machine Learning Model

Forests encompass approximately 30% of the Earth's land surface and are integral to the global carbon cycle. They store around 45% of terrestrial carbon (Bonan, 2008), predominantly in the form of Aboveground Biomass (AGB) through the process of photosynthesis. AGB comprises all live vegetation components above the ground, including stems, branches, bark, seeds, flowers, and foliage, with approximately 50% of its dry mass constituted by carbon. The measurement of AGB is typically expressed in metric tons per hectare, either as dry matter (t ha^{-1} or Mg ha^{-1}) or as carbon content (t C ha^{-1} or Mg C ha^{-1}) (Rodriguez-Veiga et al., 2017).

Intergovernmental organizations and international agreements, such as the United Nations Framework Convention on Climate Change (UNFCCC) established in 1992 and its subsequent extension through the Kyoto Protocol in 1997, have acknowledged the critical importance of monitoring and reducing greenhouse gas (GHG) emissions resulting from anthropogenic activities. At the 21st Conference of the Parties (COP21) held in 2015, a landmark comprehensive climate agreement—the Paris Agreement—was adopted, with signatory parties aiming to limit global temperature rise to below 2°C above pre-industrial levels and to pursue efforts to constrain further increase to 1.5°C . Carbon dioxide (CO_2) remains one of the most significant trace gases influencing global biogeochemical cycles, such as the carbon cycle. The increase in atmospheric CO_2 contributes to global warming and can induce changes in weather patterns (IPCC, 2014). In many tropical countries, deforestation constitutes the primary terrestrial source of CO_2 emissions and ranks as the second-largest anthropogenic source after fossil fuel combustion (Gibbs et al., 2007).

At large spatial scales, the availability of data constitutes the primary limiting factor in aboveground biomass (AGB) mapping approaches. Furthermore, estimating AGB across diverse ecosystems, such as tropical and boreal forests, presents significant challenges when applying a uniform methodology. This difficulty arises from variations in forest structure, species composition, wood density, allometric relationships, atmospheric effects, and vegetation moisture content (Rodriguez-Veiga et al., 2017).

1. Specific Data

The preprocessing of remote sensing data from various sources, which are available and sensitive to forest inventory plots, was conducted to ensure data quality and consistency. The datasets were prepared through mosaicking, georeferencing, and resampling pixels to a spatial resolution of 30 meters. Additionally, the projection was standardized to the geographic coordinate system (WGS 1984). In this study, all variables derived from different sources are summarized in Table 1.

Table 1. the variables used for quantifying the AGB by using machine learning approaches

Remote sensing dataset	Descriptions	Reference
SAR-L band backscatter intensity	The intensity of HV backscatter is strongly related to <i>AGB</i> , whereas L band SAR is associated with biomass increasing until the saturation point (approximately 150-200 t·ha ⁻¹)	Baker <i>et al.</i> , 1992; Saatchi <i>et al.</i> , 2007; Lucas <i>et al.</i> , 2010
SAR-C band backscatter intensity	The backscatter of C-band in the dry season image has the potential to discriminate within the very low biomass.	Luckman <i>et al.</i> , 1997
SAR-C band Coherence	C-band coherence (with a short repeat pass interval) has the potential to retrieve stem volume.	Gaveau <i>et al.</i> , 2001; Wagner <i>et al.</i> , 2003; Santoro <i>et al.</i> , 2018
Biophysical parameter LAI, fapar, fcover	The biophysical parameter interacted with the canopy structure.	Saatchi <i>et al.</i> , 2011; Pizaña <i>et al.</i> , 2016
SRTM (Elevation, Slope, Aspect)	The elevation, slope, and aspect are related to the forest types, species composition, and moisture.	Saatchi <i>et al.</i> , 2011; Baccini <i>et al.</i> , 2012; Hu <i>et al.</i> , 2016
%Tree cover LANDSAT VCF	The dense forest tends to have a high intensity of <i>AGB</i> .	Santoro <i>et al.</i> , 2011; Rodriguez-Veiga <i>et al.</i> , 2016; Minh <i>et al.</i> , 2018
Land surface temperature	It relates to the elevation and forest types.	Baccini <i>et al.</i> , 2012

Remote sensing dataset	Descriptions	Reference
NDVI	NDVI is a good indicator of green biomass in the deciduous and dry forest.	Foody <i>et al.</i> , 2003; Freitas <i>et al.</i> , 2005 ; Hu <i>et al.</i> , 2016 ; Su <i>et al.</i> , 2016
Wildfire (Fire frequency map)	<ul style="list-style-type: none"> -Wildfire has supported the seed germination of <i>Molinia</i> spp. in European heathland. -Some trees are not the fire-tolerance species, such as <i>Pinus spp.</i> in Thailand. -Wildfire could change the forest type from evergreen to deciduous forest type, and it can control the species composition. Furthermore, the frequently burned site has higher gross nutrient losses. 	Brys <i>et al.</i> , 2005; Wanthongchai <i>et al.</i> , 2008
Forest types	-Forest species composition and its relation to wood density.	Chave <i>et al.</i> , 2009
Forest inventory plots	-Forest plots surveyed between 2010-2016	Department National Parks, Wildlife and Plant Conservation (DNP); Thailand

2. Data analysis

The environmental variable maps, generated following the pre-processing procedures, were utilized as predictor variables. Initially, all datasets served as predictors in constructing the preliminary Aboveground Biomass (AGB) model using machine learning techniques, specifically MaxEnt and Random Forest (RF) models. Subsequently, the percentage contribution values were assigned to determine the most suitable datasets for use as predictors in the final model. The key steps of this study are illustrated in Figure 2 and are described in detail within each main section.

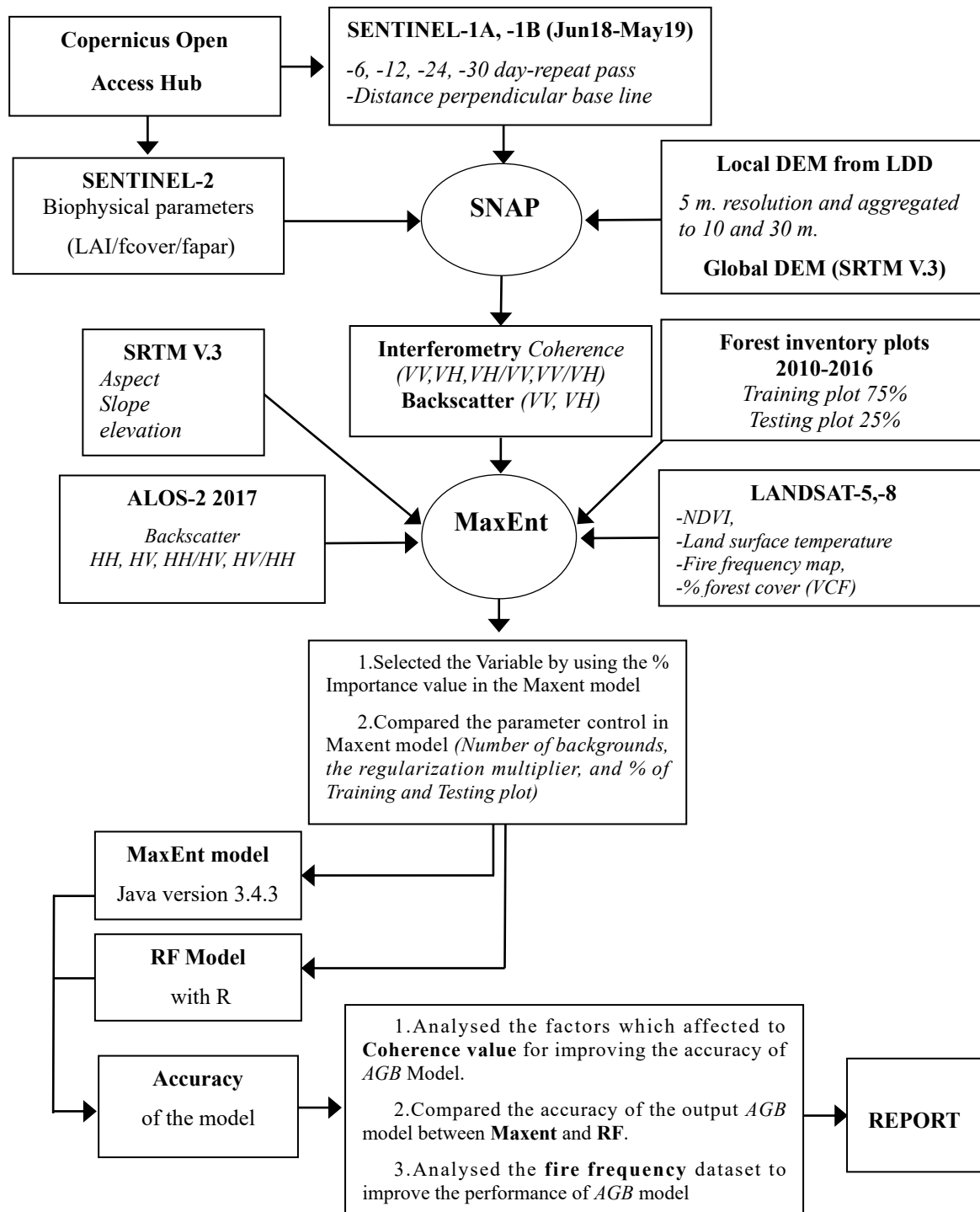


Figure 1. The flowchart of the methodology to analyse AGB mapping in this study.

3. BIOMASS OF THE TERRESTRIAL ECOSYSTEM

As previously discussed, ongoing concerns revolve around the extent to which global warming influences the release of CO₂ into the atmosphere. Consequently, scientists are increasingly interested in quantifying the biomass of forested regions to better understand, relative to a specific area, (1) the amount of biomass stored and (2) the total carbon sequestered within global forests (West, 2009). This study therefore emphasizes the biomass of woody plants, with 'biomass' defined as:

The renewable organic matter over time, known as woody biomass, encompasses the accumulated mass of roots, wood, bark, and leaves from both living and dead woody shrubs and trees. It is primarily composed of carbohydrates and lignin produced through the photosynthetic process (Hubbard, 2007).

Understanding terrestrial biomass is crucial in addressing and managing global warming. Accurate knowledge of biomass distribution across different regions is essential for enhancing our comprehension of the global carbon cycle, as biomass acts both as a source and sink of carbon, facilitating exchange with other carbon pools. Specifically, this information enables the calculation of carbon emissions resulting from deforestation and allows for the assessment of spatial changes in biomass over time. This is particularly relevant in tropical forests, where inventories have been conducted; however, many regions remain underrepresented due to incomplete, outdated, or missing data (Houghton, 2005). Despite these efforts, quantifying biomass continues to be challenging due to uncertainties related to deforestation rates and biomass density in tropical areas (Houghton, 2009).

The uncertainty surrounding the evaluation of biomass data is further worsened because direct investigation of biomass C stocks from remotely sensed data is often either impossible due to a lack of data or cannot be performed for other reasons (Barbosa 2014). A possible explanation is that current remote sensing technology cannot directly measure the girth of a tree or identify the carbon stored in parts of a tree such as the trunk, branches, and roots. Additionally, field measurements are necessary to develop estimation models. This uncertainty is an inevitable result of any data related to various areas and the study of the carbon stock model. Analyzing sources of uncertainty could lead to improvements in the overall accuracy and precision of the developing

model, enabling these tools to be better employed and prioritized in future studies (GOFC-GOLD, 2016). Future research may modify these models, for example, by adding more suitable variables to improve biomass estimation. The causes of errors encountered are summarized in Table 3. The aboveground biomass map should also indicate uncertainty (Saatchi, 2011; Rodrigues-Veiga, 2016) because uncertainty reflects the lack of knowledge of the true value, which can be represented by the range and likelihood of possible values (Eggleston, 2006).

An analysis of the source of uncertainty could lead to improvements in the overall accuracy and precision of the developing model, and thereby allow such tools to be better employed and prioritised in future studies (GOFC-GOLD, 2016) because the later researcher could modify or add more suitable variables to improve the accuracy of the biomass model.

Table 1. Sources of uncertainty in quantifying biomass maps (Foody *et al.*, 2003; Rocchini *et al.*, 2013; Gonzalez., 2014 and Avitabile *et al.*, 2016).

Type of Uncertainty	Sources of Errors
Remote Sensing Data	-Radiometric Error (Atmospheric Effect) -Geometric Error (Location and Boundary)

Type of Uncertainty	Sources of Errors
	<ul style="list-style-type: none"> -The Cartographic and Thematic Standard (The Minimum Mapping Unit (MMU) and The Definition of Land Category) -Attribute Error (Human Error, Misclassification due to the Spectral Mixture and Training Stage)
Field Measurement	<ul style="list-style-type: none"> -Error of the Tree Allometric Equation, Wood Density, and Carbon Fraction Value -Sampling Design, Plot Size, Geolocation (Depending on the Spatial Correlation and Budget), and Topography -Tree Measurement
Spatial Mismatch of Dataset	<ul style="list-style-type: none"> -Error in the Different Scales Between the Pixel Size of the Image and the Plot Size on the Ground. -Data Compatibility (the Combination of Data of Different Qualities and Sources)
Temporal Mismatch of Dataset	<ul style="list-style-type: none"> -The Seasonal Differences between Ground-Based and Space-Based Data.
Equation/Model	<ul style="list-style-type: none"> -Errors Caused by Model Residuals, Parameters, and Predictors.

Table 2. Advantages and disadvantages of each remote sensing approach to quantify the AGB in forested areas (Gibbs *et al.*, 2007; Barbosa *et al.*, 2014; Sinha *et al.*, 2015)

Method	Advantages	Disadvantages	Uncertainty
Optical	<ul style="list-style-type: none"> • Some data is free of charge 	<ul style="list-style-type: none"> • Limitation in relation to weather conditions 	High

Method	Advantages	Disadvantages	Uncertainty
SAR	<ul style="list-style-type: none"> • Suitable for simple or homogeneous forest 	<ul style="list-style-type: none"> • Cannot penetrate through the canopy of forested area • Saturation in low biomass 	Medium
	<ul style="list-style-type: none"> • InSAR and Pol-InSAR techniques are suitable for heterogeneous forest • All-weather/day-and-night capability • Penetrates through vegetation, soil, sand and dry snow • Sensitivity to polarisation and wavelength • Sensitivity to surface roughness, dielectric properties and moisture 	<ul style="list-style-type: none"> • Uncertainty at different stages • Complex process and deification • Saturated depending on wavelength • Expensive 	
LiDAR	<ul style="list-style-type: none"> • Overcomes the saturated value • Higher accuracy in predicting biomass and low RMSE 	<ul style="list-style-type: none"> • High cost per area • Restricted by the cloud • Unavailability of a large-area dataset • Lack of historical data for temporal analysis 	Low to medium

The primary function of Synthetic Aperture Radar (SAR) sensors is to penetrate forest canopies and interact with various tree components, with the interaction dependent on the sensor's wavelength. High-frequency sensors are generally limited to capturing information from the upper canopy layers, whereas low-frequency sensors possess the ability to penetrate deeper into the canopy and even reach the ground. This is because longer wavelengths tend to penetrate vegetation more effectively than shorter wavelengths (Blazter, 2001). Consequently, SAR imagery provides valuable insights into canopy volume, enabling the estimation of parameters

such as biomass magnitude, annual biomass increment, and the vertical distribution of biomass (Le Toan, 2002). However, a notable limitation is the saturation of SAR backscatter intensity at low biomass levels, which hampers accurate biomass estimation in such conditions (Koch, 2010). The saturation response varies across different forest ecosystems and is influenced by factors including wavelength, sensor polarization, energy attenuation within the canopy, canopy density, stem density, forest type, and soil conditions (Lu, 2006; Mitchard et al., 2009). These interactions collectively inform the development of predictive models for forest biomass estimation.

Table 3. The saturation point of SAR backscatter is categorized by forest biome and wavelength

Biome	Wavelength	Saturation level (t ha ⁻¹)	Reference
Temperate	C (3.8–7.5 cm)	Less sensitive – 20	Dobson <i>et al.</i> (1992), Imhoff (1995b)
	S (7.5–15 cm)	< 100	Ningthoujam <i>et al.</i> , 2016
	L (15–30 cm)	40–100	Dobson <i>et al.</i> (1992), Imhoff (1995b)
	P (30–100 cm)	100–200	Dobson <i>et al.</i> (1992), Imhoff (1995b)
	VHF	440–550	Le Toan <i>et al.</i> (2001)
Boreal	C (3.8–7.5 cm)	40	Fransson and Israelsson (1999)
	L (15–30 cm)	70–90	Fransson and Israelsson (1999), Peregon and Yamagata (2013)
	VHF	625	Fransson <i>et al.</i> (2000)
	LiDAR	No limit	Naesset, 2007
Tropical	C (3.8–7.5 cm)	20–50	Imhoff (1995a), Luckman <i>et al.</i> , 1997
	L (15–30 cm)	40–150	Imhoff (1995a), Luckman <i>et al.</i> , 1997, Lucas <i>et al.</i> , 2010, Mitchard <i>et al.</i> , 2009,
	P (30–100 cm)	300	Imhoff (1995a)

3. Active sensors and future missions

For over three decades, active sensors have been utilized in space missions, providing valuable data across diverse scientific and practical applications. Over this period, numerous missions have successfully contributed to various fields, demonstrating the significant advantages of Synthetic Aperture Radar (SAR) sensors. Notably, short-wavelength X-band sensors, approximately 3 centimeters in wavelength—such as those on TerraSAR-X and the COSMO-SkyMed constellation, which includes four polar-orbiting satellites namely CSG-1, Paz, and KOMSAT-5—continue to operate effectively. These satellites persist in delivering data in response to evolving user demands, underscoring their continued relevance and utility in space-based remote sensing.

The C-band Synthetic Aperture Radar (SAR) satellite missions, operating at approximately 5 cm wavelength, have been implemented to provide valuable data to users. Notable programs include the RADARSAT constellation and SENTINEL-1A/B. Under European Space Agency (ESA) supervision, a new series of C-band missions is planned, with SENTINEL-1C scheduled for launch in 2022. Additionally, the S-band SAR mission, NovaSAR-S, successfully conducted its operations in 2018.

The long-wavelength Synthetic Aperture Radar (SAR), specifically the L-band (~24 cm), is effective in detecting high levels of above-ground biomass (AGB). Earth observation data will continue to be collected using the ALOS-2 satellite along with two Argentinian satellites, SAOCOM-1 and SAOCOM-2. Furthermore, the European Space Agency (ESA) has planned the BIOMASS mission, scheduled for launch in 2022, which will employ P-band (435 MHz) wavelengths with multi-baseline interferometric and fully-polarimetric capabilities. This mission is expected to provide unprecedented sensitivity to AGB in forested areas by enabling the retrieval of biomass information from beneath the forest canopy. The BIOMASS mission aims for a spatial resolution of 200 meters, with a target relative Root Mean Square Error (RMSE) of less than 20% for AGB values exceeding 50 tonnes per hectare, and an RMSE of less than 10% for AGB below 50 tonnes per hectare (Banda et al., 2020).

For spaceborne LiDAR profiling sensors, three key missions—namely ICESat-1 (GLAS), ICESat-2 (ATLAS), and GEDI—have the potential to provide global tree height data essential for aboveground biomass (AGB) mapping. Additionally, LiDAR profiling can effectively extract

ground surface elevation and canopy cover when the LiDAR footprints are measured. The forthcoming LiDAR mission, the Multi-footprint Observation LiDAR and Imager (MOLI), operated by JAXA, is scheduled to launch in 2027. Consequently, integrating spaceborne LiDAR data can significantly enhance the accuracy of AGB models and reduce uncertainties in AGB estimations at a global scale.

Table 4. The mission of active remote sensing has been operational since 1991, and present and planned missions are expected to continue operating in the near future.

Satellite/ Sensors	Country/ Organization	Time span	Band/ Wavelength (cm)	Polarization	Spatial resolution (m)	Revisit (days)
ERS-1	Europe/ESA	1991-2000	C-band/5.6	VV	26	3-176
JERS-1	Japan/JAXA	1992-1998	L-band/23.5	HH	18	44
ERS-2	Europe/ESA	1995-2001	C-band/5.6	VV	26	3-176
RADARSAT-1	Canada/CSA	1995-2013	C-band/5.6	HH	8-100	3-24
ENVISAT/ASAR	Europe/ESA	2002-2012	C-band/5.6	Single, Dual	30-1000	35
ALOS-1/PALSAR	Japan/JAXA	2006-2011	L-band/23.6	Single, Dual, Quad	10-100	46
RADARSAT-2	Canada/CSA	2007-now	C-band/5.6	Single, Dual, Quad	3-100	24
TerraSAR-X	Germany/DLR	2007-now	X-band/3.1	Single, Dual Interferometric	1-18.5	11
TanDEM-X	Germany/DLR	2010-now	X-band/3.1	Dual, Quad	12	
COSMO-SkyMed -1,-2,-3,-4	Italy/CSK	2007-now 2007-now 2008-now 2010-now	X-band/3.1	Single, Dual	1-100	16/1 (4satellites)
RISAT-1	India/ISRO	2012-	C-band/5.6	Single, Dual, Quad	1-50	25
KOMSAT-5	Korea/KARI	2013-	X-band/3.2	Dual/Quad	1-20	28
ALOS-2/PALSAR-2	Japan/JAXA	2014-now	L-band/23.8	Single, Dual, Quad	1-100	14
SENTINEL-1A SENTINEL-1B SENTINEL-1C	Europe/ESA	2014-now 2016-now	C-band/5.6	Single, Dual, Quad	9-15	12/6 (2satellites)
SAOCOM-1A SAOCOM-1B	Argentina/CONAE	2018-now 2020-now	L-band/	Quad	7-100	16/8 (2satellites)
PAZ	Spain/CDTL	Feb22,2018	X-band/3.1	Single, Dual	1-16	11
NovaSAR-1	U.K./UKSA	Sep17,2018	S-band/9.4	Dual, Tri-pol (HH+VV+HV)	6-45	14
RADARSAT Constellation	Canada/CSA	Jun12,2019	C-band/5.6	Single, Dual, Quad	1-100	12
CSG-1	Italy/CSG	2019-now	X-band/	Single, Dual, Quad	0.8-40	16
CSG-2	Italy/CSG	Jan31,2022	X-band/	Single, Dual, Quad	0.8-40	16
NISAR	USA/NASA, ISRO	Jul 30,2025	L-band/24 S-band/9	Quad	3-10	12



Satellite/ Sensors	Country/ Organization	Time span	Band/ Wavelength (cm)	Polarization	Spatial resolution (m)	Revisit (days)
MOLI	Japan/JAXA	Plan 2027	LiDAR/Imager	Multi-footprint	25	-
ALOS-4/PALSAR-3	Japan/JAXA	Jul1,2024	L-band/23.8	Dual, Quad	3-10	14
BIOMASS	Europe/ESA	Apr29,2025	P-band/69.0	Quad	50	25-45
TanDEM-L	Germany/DLR	plan 2028	L-band/23.6	Single, Dual Interferometric	-	16
TerraSAR-X2	Germany/DLR	plan	X-band/3.1	Full dual, Quad	0.25-50	-

Single = single polarization, Dual = dual polarization, Quad = quad polarization

4. ABOVEGROUND BIOMASS ESTIMATION APPROACHES

There are multiple methodologies for extrapolating sampled plots to generate a comprehensive gridded map for biomass estimation. Given that it is unfeasible to measure every individual tree across entire forested regions, the integration of remote sensing data with forest sampling plots presents a viable and effective approach to mapping above-ground biomass (AGB). Currently, various methods have been developed for AGB prediction, which can be categorized into two primary types: 1) parametric algorithms and 2) non-parametric algorithms (Lu et al., 2016). Within the parametric category, approaches can be further subdivided into empirical regression models and semi-empirical or physical-based models (Santoro & Cartus, 2018).

4.1 Parametric algorithm

The parametric model is based on the relationship between the dependent variable (i.e., the amount of biomass) and independent variables (i.e., remote sensing datasets and auxiliary datasets).

Parametric empirical regression model

Empirical regression techniques, including both simple linear and multiple regression models, have been widely employed in numerous studies (Ranson et al., 1997; Santos et al., 2003; Foody et al., 2003; Sun et al., 2011). The regression algorithm is straightforward and facilitates the computation of the slope coefficient and intercept using a set of training plots. However, the

assumption of a linear relationship between radar backscatter intensity and biomass values often leads to underestimation or overestimation of actual biomass (Santoro & Cartus, 2018). Moreover, the multiple regression approach presumes that the independent variables—primarily features derived from remote sensing datasets—are not correlated with the dependent variable (field-measured above-ground biomass, AGB). This assumption may limit the model's predictive accuracy and overall effectiveness (Liang & Wang, 2012).

Parametric semi-empirical and physical-based model

Regarding approaches that do not require training plots for AGB mapping estimates, the physics-based model can operate based on the relationship between SAR images and the magnitude of AGB or GSV (Quegan et al., 2017; Santoro & Cartus, 2018). The parameters used to build this model can determine the backscatter intensity (i.e., Water Cloud Model; WCM) (Peregon & Yamagata, 2013) and the coherence value (Interferometric Water Cloud Model; IWCM) (Santoro et al., 2005) of SAR observations. However, the semi-empirical model necessitates a dataset of forest GSV measurements to estimate coefficients across different forest ecosystems (Santoro et al., 2002). Additionally, the coefficient constants depend on factors such as the dielectric constant in the vegetation, forest structure, and seasonal conditions (Pulliainen et al., 1996; Santoro et al., 2002). This method has been successfully used to estimate the AGB in the northern biome, with applications in Siberia, Scandinavia, and Northeast China (Santoro et al., 2006). Moreover, for global AGB mapping (Globbiomass), the physics-based model is a valuable approach for quantifying forest biomass since it does not necessarily rely on forest sample plots (Santoro et al., 2018b). Nevertheless, this approach has not been tested across all forest ecoregions (Quegan et al., 2017) for verifying experimental coefficient values. Additionally, a study by Peregon and Yamagata (2013) found that the WCM model tends to underestimate in dense forests with high biomass levels, due to SAR signal saturation.

4.2 Non-parametric algorithm

The relationship between forest biomass and variables derived from remote sensing datasets has not been consistently modeled using linear equations (Song, 2013). Often, the correlation between these entities is complex, rendering parametric approaches unsuitable for predicting above-ground biomass (AGB) distribution models (Lu et al., 2016). Consequently,

machine learning methods have gained increasing popularity for estimating AGB, as they leverage mathematical models trained on patterns identified in existing data (Hackeling, 2014; Ghatak, 2017). These approaches effectively address issues arising from non-linear relationships between predictor variables and in-situ measurements. For example, Hayashi et al. (2019) demonstrated that machine learning models, such as Random Forest (RF), could overcome saturation effects observed at AGB levels up to 280 Mg ha⁻¹ when utilizing time-series datasets of ALOS-2 backscatter intensity. Similarly, Englhart et al. (2012) found that artificial neural networks (ANN) are well-suited for multi-temporal analysis of synthetic aperture radar (SAR) data to generate accurate AGB maps and distinguish between low and high biomass regions. Nevertheless, implementing such models requires adequate training and testing datasets, which is often hampered by the scarcity of in-situ data in tropical forests for calibration and validation purposes (Cartus & Santoro, 2019; Quegan et al., 2017). Literature indicates that non-parametric, tree-based approaches—such as those employed by Baccini et al. (2008)—and Maximum Entropy (MaxEnt) models (Saatchi et al., 2008) have been successfully used to estimate biomass at regional scales in tropical forests. Santoro and Cartus (2018) also noted that the use of SENTINEL-1 data, with 6- and 12-day revisit intervals, for coherence-based AGB modeling under varying weather conditions has yet to be thoroughly explored.

4.3 MaxEnt Implementation

The MaxEnt software is highly user-friendly, allowing for easy modification of parameter settings, which has contributed to its adoption as a standard tool for species distribution modeling (Halvorsen, 2013). In this study, multi-source remote sensing datasets were prepared for analysis using the MaxEnt algorithm, as illustrated in Figure 1. These datasets included various types of data extracted from optical and microwave sensors, such as biophysical parameters (LAI, FCover, FPar), forest cover percentage (Vegetation Continuous Field; VCF product), forest fire frequency maps, aspect, and slope of the study area. All prediction grids were resampled to a uniform spatial resolution of 20 meters, ensuring consistent grid dimensions and geographic coordinates across the datasets.

The forest inventory plots within the study area were provided by DNP. The mean aboveground biomass was calculated at 146 t·ha⁻¹, with a range spanning from 1.0 t·ha⁻¹ to 485

t·ha⁻¹. The plots were categorized into biomass classes at 50 t·ha⁻¹ intervals, specifically: 0-50, 50-100, 100-150, 150-200, and greater than 200 t·ha⁻¹. Subsequently, each biomass class was subdivided into two groups: one used for model training, comprising 80% of the total plots, and the other for validation, comprising the remaining 20%.

The parameter controls within the MaxEnt algorithm are used to identify the most influential variables by evaluating the Area Under the Curve (AUC) metric. The AUC value ranges from 0 to 1, where a value of 1 indicates perfect discrimination capability of the model, and a value of 0.5 suggests that the model performs no better than random chance (Heinaneen et al., 2012).

All predictor variables derived from multi-source datasets were modeled using MaxEnt software. Critical variables were identified based on the average percentage contribution across all classes. For the quantification of aboveground biomass (AGB), predictor variables with an average importance greater than 1% were selected, while those with less than 1% were excluded from the MaxEnt modeling process. This approach ensures that only the most influential variables contribute to the model, thereby improving its robustness and reliability.

The experiment and exploration of the value for controlling the parameters in the MaxEnt software determined how to assign suitable parameter control in the MaxEnt model, which, as a result, could achieve high accuracy in AGB mapping.

This procedure began by testing the parameter controls, such as the number of background points (setting different amounts to 100, 500, 1000, 5000, 7500, 10000, 25000, 50000, 100000, and 200000 points).

The result of the suitable parameter control (the number of background points, and the regularisation multiplier value) was a fixed value to quantify *AGB* mapping with the MaxEnt model.

The MaxEnt model to calculate the probability of biomass in all classes (5 classes). It combined all classes to a single map of *AGB* by using equation1 (Saatchi *et al.*, 2011b).

$$\widehat{AGB} = \frac{\sum_{i=1}^N P_i^n AGB_i}{\sum_{i=1}^N P_i^n} \quad \text{Equation 1}$$

Where \widehat{AGB} is the *AGB* prediction per pixel, and P_i does MaxEnt calculate the probability for each *AGB* range. AGB_i is the average value within class i . The power n of the probability is used to weight the predicted value towards the maximum probability closest to the actual value when other probabilities are small. In this case, $n = 3$, as follows from Saatchi et al. (2011 b) 's study.

It combined all classes to a single map of *AGB* by using equation 1. And the uncertainty of the *AGB* prediction per pixel was analysed alongside the root mean square error (Eq. 2 and Eq. 3)

$$\varepsilon_{prediction} = \frac{\sigma_{\widehat{AGB}}}{\widehat{AGB} \times 100} \quad \text{Equation 2}$$

$$\sigma_{\widehat{AGB}} = \sqrt{\frac{\sum_{i=1}^N (AGB_i - \widehat{AGB})^2 P_i}{\sum_{i=1}^N P_i}} \quad \text{Equation 3}$$

Where: \widehat{AGB} is the *AGB* prediction per pixel, and P_i represents the probability calculated by MaxEnt for each *AGB* range. AGB_i represents the average value within class i . $\varepsilon_{prediction}$ represents the uncertainty of the prediction probability from the MaxEnt model.

The total uncertainty value can be estimated by using Equation 4 and is composed of **4 sources of uncertainty**. This equation is shown below:

$$\varepsilon_{AGB} = (\varepsilon_{measurement}^2 + \varepsilon_{allometry}^2 + \varepsilon_{sampling}^2 + \varepsilon_{prediction}^2) \quad \text{Equation 4}$$

The accuracy of the model was evaluated using aboveground biomass (*AGB*) data from the testing dataset. Approximately 20% of the sample plots, set aside specifically for accuracy assessment, were used. A scatter plot was generated between the observed aboveground biomass from field surveys (x) and the estimated aboveground biomass derived from the model (y). Statistical indicators were then calculated to assess the model's performance and accuracy, including the coefficient of determination (R^2), root mean square error (RMSE) as expressed in Equation (5), and the relative root mean square error (rRMSE) as expressed in Equation (6).

$$RMSE = \sqrt{\frac{1}{n} \sum_{i=1}^n \left(\frac{\bar{H}_d^{i,m} - \bar{H}_d^{i,c}}{\bar{H}_d^{i,m}} \right)^2} \quad \text{Equation 5}$$

$$rRMSE = \frac{\sqrt{\sum_{i=1}^n (\bar{H}_d^{i,m} - \bar{H}_d^{i,c})^2}}{\sqrt{\sum_{i=1}^n (\bar{H}_d^{i,m})^2}} \times 100 \quad \text{Equation 6}$$

Where: $\bar{H}_d^{i,m}$ means predicted *AGB* Model
 $\bar{H}_d^{i,c}$ means actual *AGB*

The reliability of the model was assessed using the relative root mean square error (rRMSE), following the criteria proposed by Despotovic *et al.* (2016).

rRMSE < 10% (Excellent)
 10% < rRMSE < 20% (Good)
 20% < rRMSE < 30% (Fair)
 rRMSE > 30% (Poor)

A lower RRMSE indicates a better model fit, while higher values suggest greater deviation between predicted and actual values.

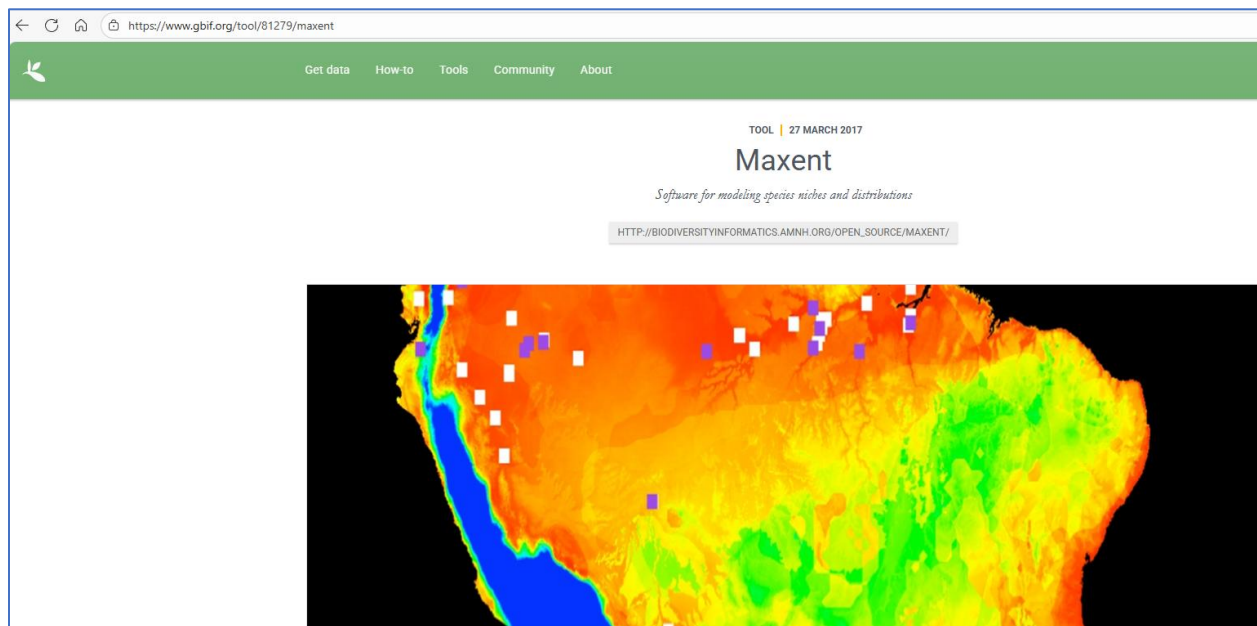
Tutorial

This tutorial is created for educational purposes and a training course at GISTDA.

Introduction

We demonstrate the application of the Maximum Entropy Model, MaxEnt (Phillips et al., 2006), for estimating the carbon stock in forested areas. The preparation of data is a crucial step, which requires understanding several software and file formats such as Microsoft Excel, ArcGIS, or QGIS. This will guide users on how to prepare data using different software before running the MaxEnt model (JAVA Version).

For more detailed instructions on how MaxEnt operates, interprets results, and adjusts the advanced options, users should visit <https://www.gbif.org/tool/81279/maxent>



Maxent is a stand-alone Java application and can be used on any computer running Java version 1.5 or later.

What is Machine learning

Machine learning encompasses the utilization of historical data and experiential information derived from practitioners to enhance performance and generate predictive insights (Mohri et al., 2018). Its applications are diverse and far-reaching. For example, the species

distribution model (SDM) employs interpolation and extrapolation techniques to analyze point observations across spatial landscapes, thereby predicting data for regions without direct sampling (Franklin, 2010).

For predicting aboveground biomass (AGB) distribution in forested regions, both parametric methods, such as regression models, and non-parametric approaches, including machine learning algorithms, can be employed to extrapolate biomass values across a grid map. These methods have been demonstrated to be effective in various studies (Saatchi et al., 2011; Baccini et al., 2012; Cartus et al., 2014; Rodriguez-Veiga et al., 2016).

This study selected two widely used machine learning algorithms for predicting aboveground biomass (AGB) due to several advantages. First, these models can integrate diverse variable types, combining continuous remote sensing data with discrete GIS datasets to effectively predict AGB distribution. Second, they provide probabilistic outputs, enabling the assessment of prediction confidence and the calculation of error at the pixel level. Third, since these algorithms are designed to operate with presence-only data, there is no need for absence data; instead, they utilize background or pseudo-absence data, such as sampling points. Fourth, the models facilitate sensitivity analysis for each predictor variable, allowing researchers to determine the influence of individual factors on AGB and identify variables that may be excluded to streamline the model. This paper outlines a project aimed at evaluating carbon sequestration in forested regions using a machine learning approach—specifically, the MaxEnt model. Although the current focus is on forestry and climate applications, the methodology is broadly applicable to other domains, such as agricultural assessments and crop yield estimation.

Aims

- To study the process of preparing data for assessing carbon accumulated in forested areas using a machine learning model.
- To assess carbon accumulated in forested areas using the Maximum entropy model.

Study site

The project utilizes an Area of Interest (AOI) for which sample plot data has been collected. The data includes:

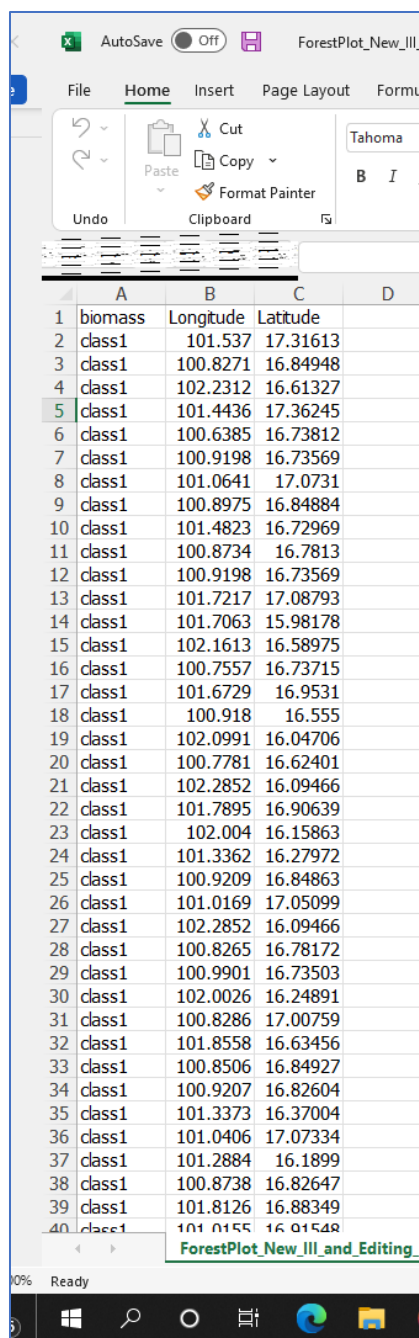
-raster_bnd: a raster file that defines the AOI boundary.

-biomass_plot: survey data from 225 sample plots collected by the Department of National Parks, Wildlife and Plant Conservation between 2010 and 2016. The coordinates are geographic, with a pixel size of approximately 40×40 metres.

- The Wtotal_ha column in the data contains the calculated biomass values in tons per hectare, which are derived from tree volume and height measurements.

-The vVolume column contains the wood volume in cubic meters for each survey plot.

For the machine learning model, the sample plot data must be randomly divided into 80% for training plots and 20% for testing plots. This data should be saved as a **.csv file** and categorized into five classes based on biomass, such as 0-50, 50-100, 100-150, 150-200, and >200 tons per hectare.



	A	B	C	D
1	biomass	Longitude	Latitude	
2	class1	101.537	17.31613	
3	class1	100.8271	16.84948	
4	class1	102.2312	16.61327	
5	class1	101.4436	17.36245	
6	class1	100.6385	16.73812	
7	class1	100.9198	16.73569	
8	class1	101.0641	17.0731	
9	class1	100.8975	16.84884	
10	class1	101.4823	16.72969	
11	class1	100.8734	16.7813	
12	class1	100.9198	16.73569	
13	class1	101.7217	17.08793	
14	class1	101.7063	15.98178	
15	class1	102.1613	16.58975	
16	class1	100.7557	16.73715	
17	class1	101.6729	16.9531	
18	class1	100.918	16.555	
19	class1	102.0991	16.04706	
20	class1	100.7781	16.62401	
21	class1	102.2852	16.09466	
22	class1	101.7895	16.90639	
23	class1	102.004	16.15863	
24	class1	101.3362	16.27972	
25	class1	100.9209	16.84863	
26	class1	101.0169	17.05099	
27	class1	102.2852	16.09466	
28	class1	100.8265	16.78172	
29	class1	100.9901	16.73503	
30	class1	102.0026	16.24891	
31	class1	100.8286	17.00759	
32	class1	101.8558	16.63456	
33	class1	100.8506	16.84927	
34	class1	100.9207	16.82604	
35	class1	101.3373	16.37004	
36	class1	101.0406	17.07334	
37	class1	101.2884	16.1899	
38	class1	100.8738	16.82647	
39	class1	101.8126	16.88349	
40	class1	101.0155	16.01548	

Figure 5. The training dataset were prepared in .csv format, including examples of plot data and the required data structure to be used for model training.

Required Software and Datasets

To prepare the necessary data and run the machine learning model, several software programs must be installed:

- **SNAP**
- **ArcGIS**
- **ENVI or QGIS**
- **Maximum entropy model (MaxEnt)**, which can be downloaded from the American Museum of Natural History website.

https://biodiversityinformatics.amnh.org/open_source/maxent/

Data preparation for quantifying forest biomass carbon stocks

The preprocessing stage was carried out to ensure that all environmental layers had identical dimensions in terms of columns and rows, which is essential for model training. **Nine specific variable factors** (datasets) to be prepared for the machine learning model. The pixel size for all data layers must be the same size at 40 metres, or approximately 0.000185 degrees, and the data must be extracted using the **raster_bnd** boundary mask. The required datasets are:

1. Remote Sensing Data Preparation

1.1 The ALOS-2 dataset can be downloaded at

https://www.eorc.jaxa.jp/ALOS/en/dataset/fnf_e.htm

Moreover, this is the link to convert the DN value to a backscatter coefficient value.

https://www.eorc.jaxa.jp/ALOS-2/en/calval/calval_index.htm

1.2 SRTM can be downloaded at <https://earthexplorer.usgs.gov/> (You should apply to get a username and password for downloading any other datasets that you desire.)

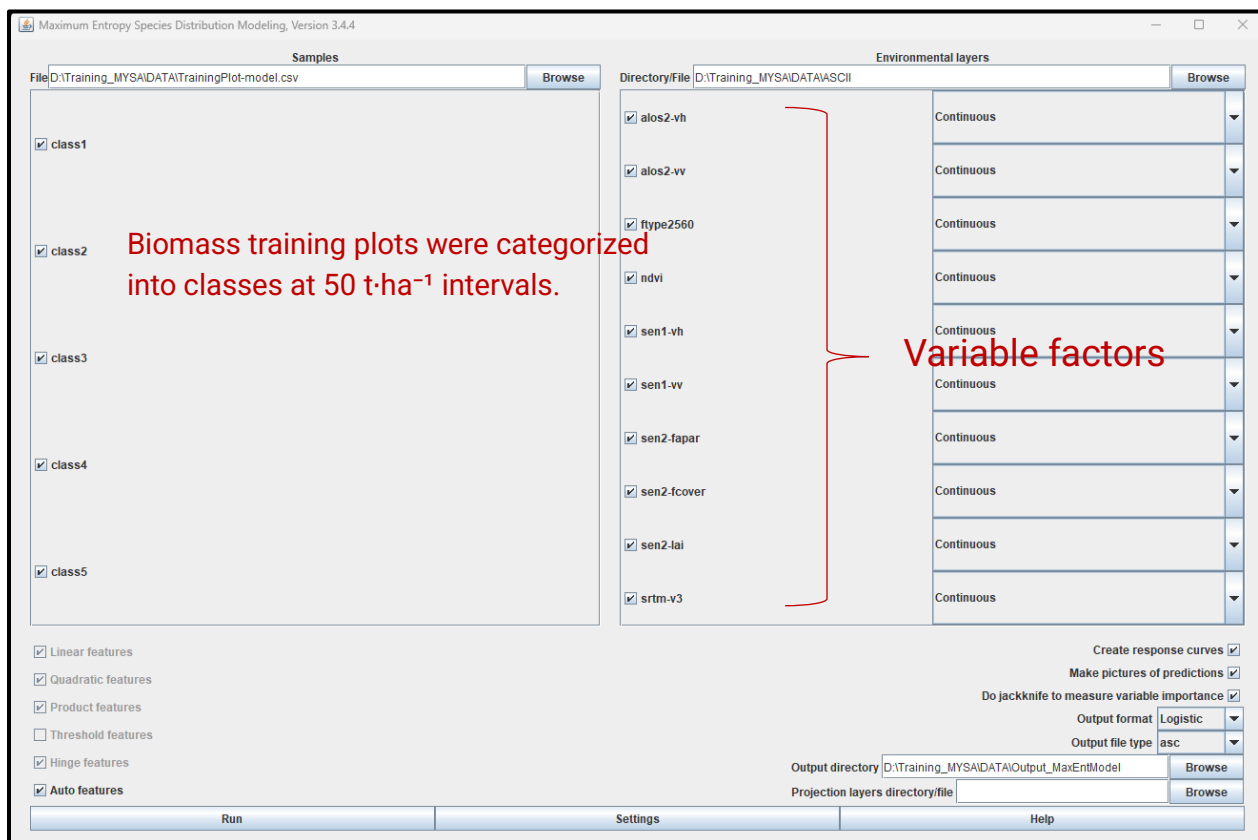
1.3 The Sentinel-2 can extract the variable factors, which relate to the magnitude of AGB, such as NDVI, LAI, FCOVER, FAPAR, etc. It can be processed using SNAP software or any other method (some datasets are available on Google Earth Engine).

1.4 SENTINEL-1 C-band

link → <https://step.esa.int/main/doc/tutorials/>

The document also provides several links for downloading data and tutorials on data preparation, including instructions on how to prepare ALOS2 data, SRTM data, and SENTINEL-2 data using SNAP, as well as a link to Sentinel-1 tutorials.

1.5 Forest type dataset retrieved from the Royal Forest Department, 2017



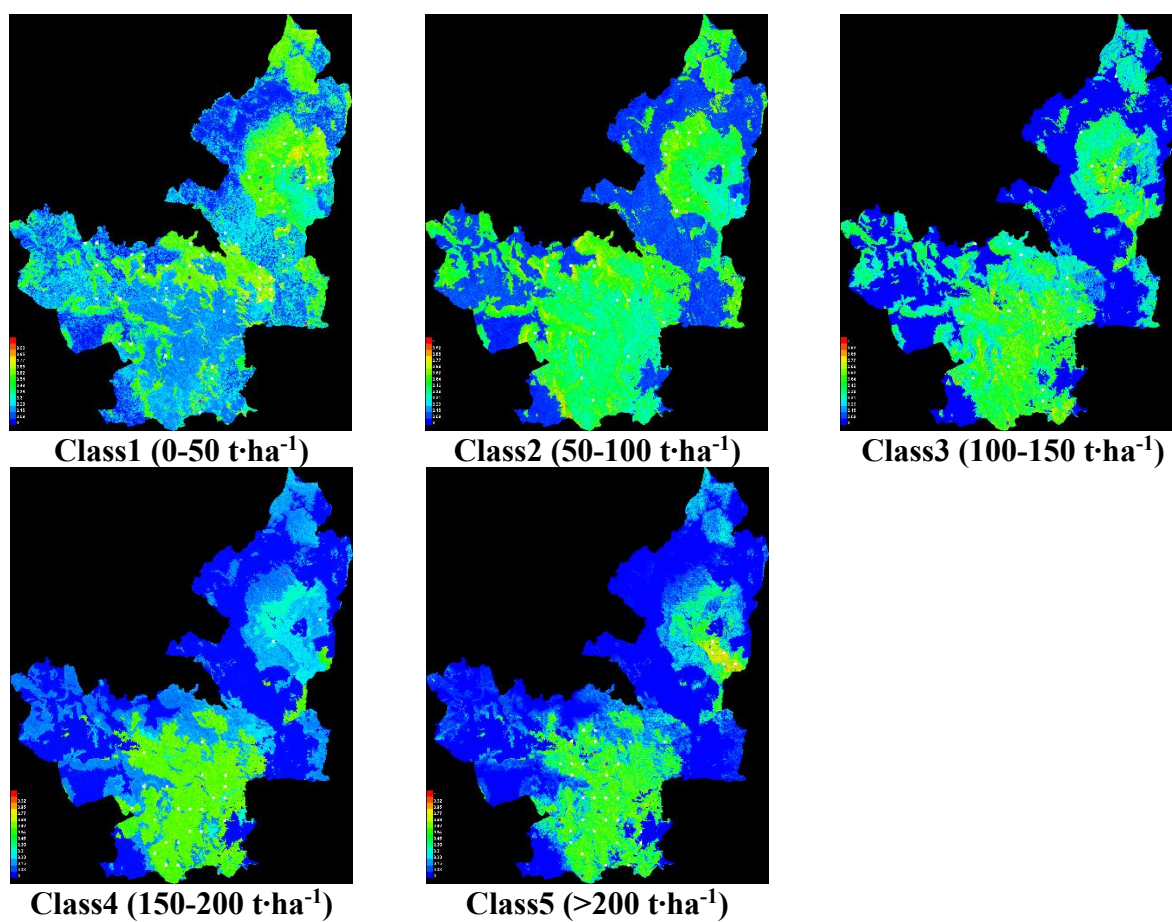


Figure 7. The probabilities of the 5 *AGB* classes resulting from the MaxEnt model.

Underfitting and Overfitting

Underfitting occurs when a model is too simple to capture the underlying structure of the data. As a result, it performs poorly not only on unseen data but also on the training data itself, indicating that the model has failed to learn the relationships between predictors and response variables adequately. Several solutions to the problem of underfitting are possible:

1. A more complex model should be constructed to improve accuracy, such as Machine learning (ML), Deep learning (DL), etc.
2. The predictor variables should be strongly related to the magnitude of AGB.

Overfitting occurs when a model learns the training data too precisely, including noise and random fluctuations, rather than the general underlying patterns. Consequently, the model achieves high accuracy on the training data but performs poorly on unseen data, reflecting limited generalization ability. Several solutions to the problem of overfitting are possible:

1. Try a simpler model (linear instead of polynomial regression, or SVM with a linear kernel instead of RBF, a neural network with fewer layers/units).
2. Reduce the dimensionality of examples in the dataset.
3. Add more training data, if possible.
4. Regularize the model.

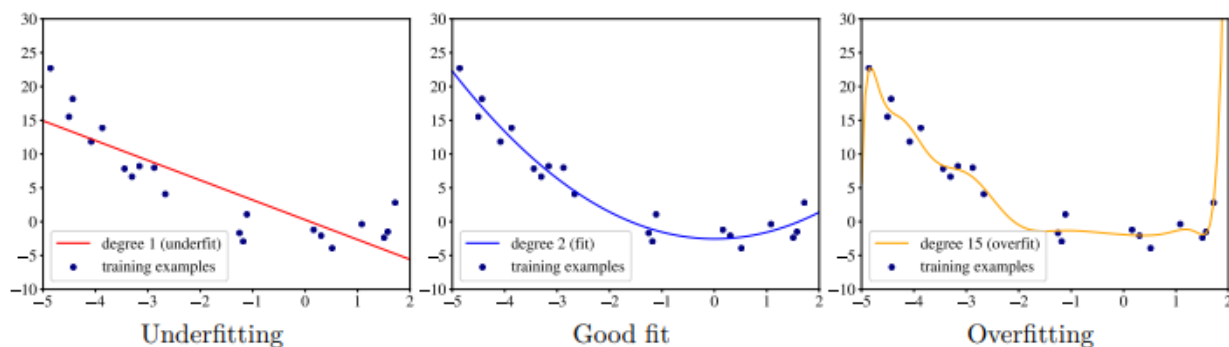


Figure8. Examples of underfitting (linear model), good fit (quadratic model), and overfitting (polynomial of degree 15). (source: Andriy Burkov : The Hundred-Page Machine Learning Book)

Forest resource inventory technique for quantifying AGB in forested area

Forest inventory is a critical procedure for collecting field data, serving as a representative sampling method to develop models of aboveground biomass (AGB). In the case of extensive forested areas, stratification enhances the efficiency of sampling by determining the appropriate number of sample plots based on aboveground biomass density. When foundational data is available—such as forest type maps, AGB datasets, or forest canopy density (FCD)—these resources can be effectively utilized to plan and stratify forest resource surveys.

This is a tutorial to calculate the optimal number of forest plots that apply for following Winrock International's CDM A/R sample plot calculator spreadsheet tool.

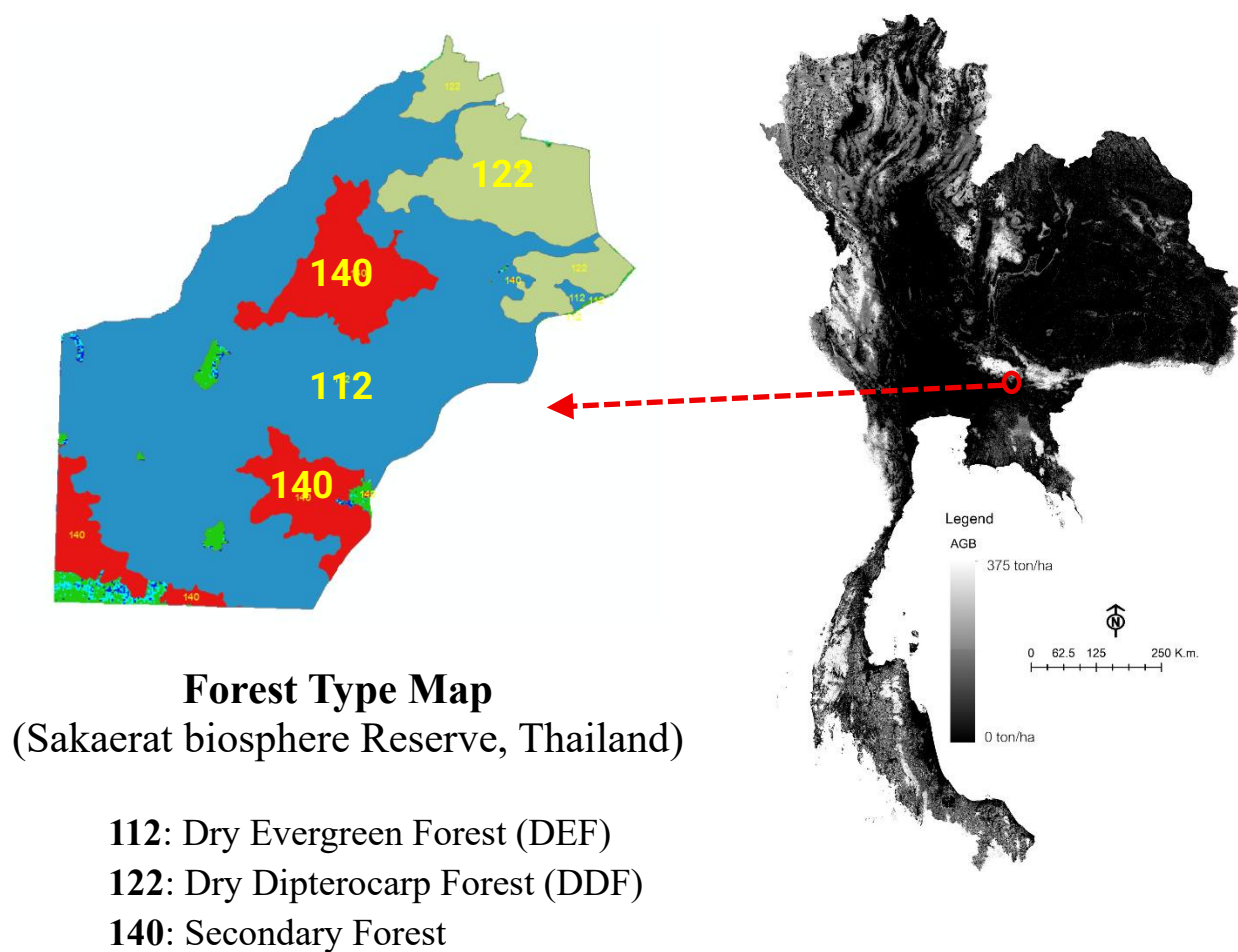
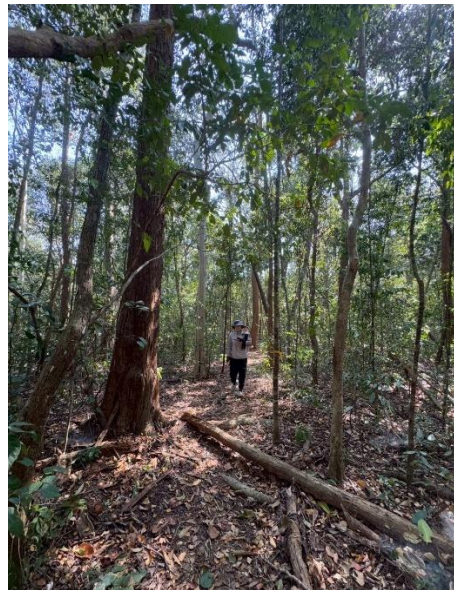


Figure 9. Forest type map over Sakaerat biosphere reserve, Nakhonrachasima province, North-eastern of Thailand



Wet season



Dry season

a. Dry evergreen



Wet season



Dry season

b. Dry dipterocarp

Figure 10. The forest types in Sakaerat biosphere reserve, Nakhonrachasima province, North-eastern of Thailand are comprised of Dry evergreen forest and Dry dipterocarp forest.

Forest Types and Ecological Characteristics

The Sakaerat Biosphere Reserve, situated in Nakhon Ratchasima Province in Northeastern Thailand, encompasses two primary forest types, each characterized by distinct ecological and biomass properties:

1. Dry Evergreen Forest (DEF) – This forest type is distinguished by relatively moist conditions and a diverse assemblage of tree species that retain their leaves year-round. The persistent canopy facilitates continuous photosynthesis, thereby supporting consistent aboveground biomass accumulation. Additionally, the rarity of wildfires in DEF contributes to biomass preservation and enhances long-term carbon sequestration capacity.

2. Dry Dipterocarp Forest (DDF) – Conversely, DDF undergoes complete leaf shedding during the dry season, resulting in seasonal fluctuations in canopy cover and photosynthetic activity. This forest is susceptible to annual wildfires, which can cause substantial biomass loss and alter carbon cycling dynamics. The recurrent disturbance from fires influences species composition, stand structure, and the spatial distribution of biomass within the forest.

These contrasting ecological processes significantly impact the spatial distribution and temporal variability of aboveground biomass in the reserve. Consequently, understanding these differences is crucial for informing sampling design, biomass estimation, and the development of long-term carbon monitoring strategies.

Forest type map (RFD, 2018)

Code	Forest type
112	Dry evergreen forest; DEF
122	Dry dipterocarp forest; DDF
140	Secondary forest; SF

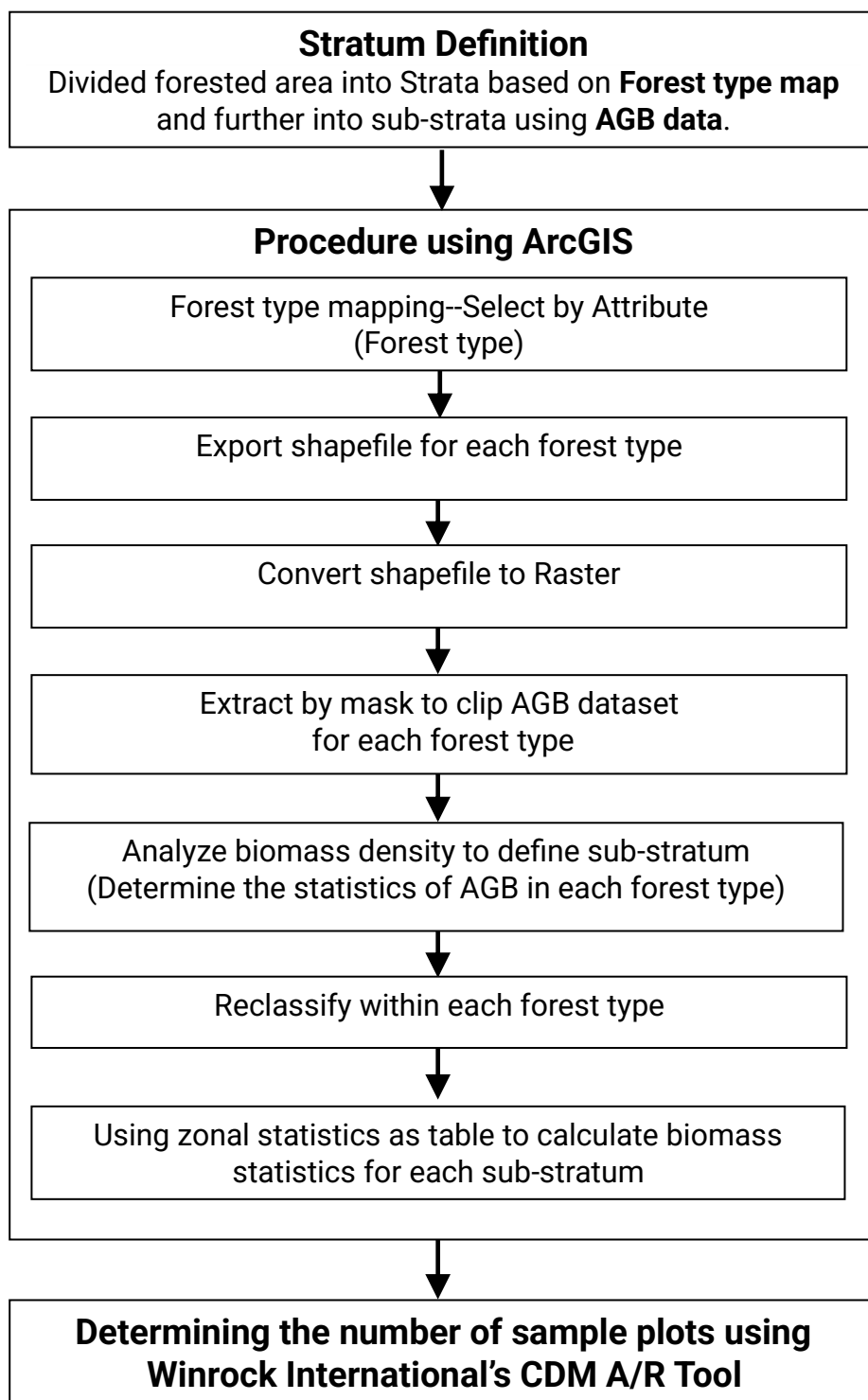


Figure 11. Flowchart of stratification to calculate the number of sampling plots for forest resource inventory.

Aboveground Biomass Map were sourced from GISTDA (2022), with a spatial resolution of 20 meters per pixel (equivalent to 0.04 ha). AGB values were extracted and analyzed using ArcGIS software, specifically the “Zonal Statistics as Table” function.

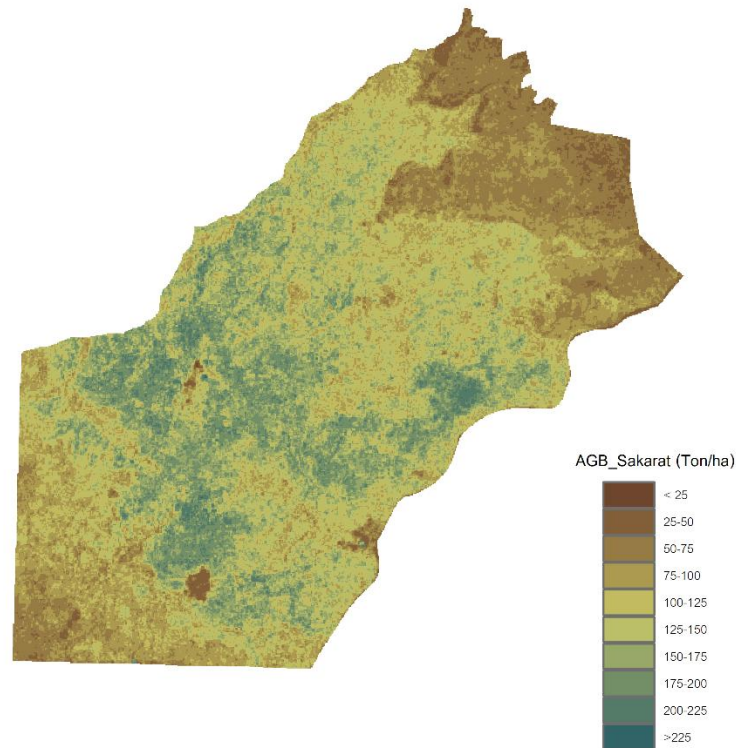


Figure 12. Above-ground biomass map of Sakaerat biosphere Reserve Forest within study site.

If you do not have *AGB* mapping to calculate the number of sampling plots, you can use the forest above-ground biomass at a large-scale map (Global scale), such as the ESA CCI and the JPL 2020 Global Biomass dataset.

Source of AGB datasets (Global scale)

The AGB datasets can be used to analyze the optimal number of forest plots, followed by Winrock International's CDM A/R sample plot calculator spreadsheet tool.

1. ESA CCI Global Forest Above Ground Biomass https://gee-community-catalog.org/projects/cci_agb/

This dataset, updated to v5.01, provides estimates of forest above-ground biomass for the years 2010, 2015, 2016, 2017, 2018, 2019, 2020, and 2021. The data products consist of two (2) global layers that include estimates of:

- Above-ground biomass (AGB, measured in tons per hectare, i.e., Mg/ha) (raster dataset). It is defined as the oven-dry weight of the woody parts—including stem, bark, branches, and twigs—of all living trees, excluding stumps and roots.

- Per-pixel estimates of above-ground biomass uncertainty expressed as the standard deviation in Mg/ha (raster dataset)

ESA CCI Global Forest Above Ground Biomass

https://gee-community-catalog.org/projects/cci_agb/

This dataset updated to v5.01 provides estimates of forest above-ground biomass for the years 2010, 2015, 2016, 2017, 2018, 2019, 2020 and 2021.

The data products consist of two (2) global layers that include estimates of:

1. **Above ground biomass** (AGB, unit: tons/ha i.e., Mg/ha) (raster dataset). This is defined as the mass, expressed as oven-dry weight of the woody parts (stem, bark, branches and twigs) of all living trees excluding stump and roots
2. Per-pixel estimates of **above-ground biomass uncertainty** expressed as the standard deviation in Mg/ha (raster dataset)



Earth Syst. Sci. Data, 13, 3927–3950, 2021
https://doi.org/10.5194/essd-13-3927-2021
© Author(s) 2021. This work is distributed under the Creative Commons Attribution 4.0 License.

Earth System
Science
Data

The global forest above-ground biomass pool for 2010 estimated from high-resolution satellite observations

Maurizio Santoro¹, Oliver Cartus¹, Nuno Carvalho^{1,2}, Daniel M. A. Rozendael^{1,3,4}, Valerio Avitabile⁵, Arnan Araza⁶, Sytae de Bruin⁷, Martin Herold⁸, Shann Quesan⁹, Pedro Rodriguez-Valm¹⁰, Heiko Balzer^{11,12}, João Carrizosa¹³, Dmitry Schepaschenko^{14,15}, Mikhail Korev¹⁶, Yasuhiro Shimada¹⁷, Takuya Ishi¹⁸, Álvaro Moreno-Martínez^{19,20}, Jara Cankovic²¹, Roberto Cazzola Gatti²², Pulama da Conceição Ribeiro²³, Nisheta Devanath²⁴, Nicolas Labrière²⁵, Jingling Liang²⁶, Jeremy Landsberg²⁷, Edward L. A. McIlrath²⁸, Alexandra Morel²⁹, Ana Maria Pacheco Pascalegani^{30,31}, Casey M. Ryan³², Ferry Slik³³, Gala Voglio-Laurin³⁴, Hans Verbeeck³⁵, Arif Wijaya³⁶, and Simon Wilcock³⁷

¹Gamma Remote Sensing, 3073 Günslingen, Switzerland
²Max Planck Institute for Biogeochemistry, Hans Knöll Strasse 10, 07745 Jena, Germany
³Departamento de Ciências e Engenharia do Ambiente, DCEA, Faculdade de Ciências e Tecnologia, FCT, Universidade Nova de Lisboa, 2829-516 Caparica, Portugal
⁴Laboratory of Geo-Information Science and Remote Sensing, Wageningen University and Research, Droevendaalsesteeg 3, 6708 PB Wageningen, the Netherlands
⁵Plant Production Systems Group, Wageningen University and Research, P.O. Box 430, 6700 AK Wageningen, the Netherlands
⁶Centre for Crop Systems Analysis, Wageningen University and Research, P.O. Box 430, 6700 AK Wageningen, the Netherlands
⁷Joint Research Centre, European Commission, Ispra, Italy
⁸National Centre for Earth Observation (NCEO), University of Sheffield, Sheffield, S3 7RH, UK
⁹Centre for Landscape and Climate Research, School of Geography, Geology and the Environment, University of Leicester, LE1 7RH, UK
¹⁰National Centre for Earth Observation (NCEO), Leicester, LE1 7RH, UK
¹¹International Institute for Applied Systems Analysis, Schlossplatz 1, 2361 Laxenburg, Austria
¹²Center of Forest Ecology and Productivity, Russian Academy of Sciences, Profsoyuznaya 84/32/14, 117997 Moscow, Russia
¹³Institute of Ecology and Geography, Siberian Federal University, 79 Svobodny Prospekt, 660041 Krasnoyarsk, Russia
¹⁴Laboratory of Ecophysiology of Permafrost Systems, V.N. Sukachev Institute of Forest of the Siberian Branch of the Russian Academy of Sciences – separated department of the KSC SB RAS, 660030 Krasnoyarsk, Russia
¹⁵Tokyo Denki University, School of Science and Engineering, Division of Architectural, Civil and Environmental Engineering, Ishizuka, Hachiyama, Hiki, Saitama, 350-0194, Japan
¹⁶Remote Sensing Technology Center of Japan, Tokyo R&D Teramom Bldg. 3F, 3-17-1 Teramom, Minato-Ku, Tokyo, 105-6501, Japan
¹⁷Image Processing Laboratory (IPL), Universitat de València, Valencia, Spain
¹⁸Numerical Terrasym Simulation Group (NTSG), University of Montana, Missoula, MT, USA
¹⁹Department of Forest Inventory and Management, Faculty of Forestry and Wood Technology, University of Zagreb, Svetosimunska cesta 23, 10000 Zagreb, Croatia
²⁰Biological Institute, Tomsk State University, 634050 Tomsk, Russia
²¹Department of Geography, School of Environment, Education and Development, University of Manchester, Oxford Road, M13 9PL, Manchester, UK
²²Guyana Forestry Commission, 1 Water Street, Kingston, Georgetown, Guyana

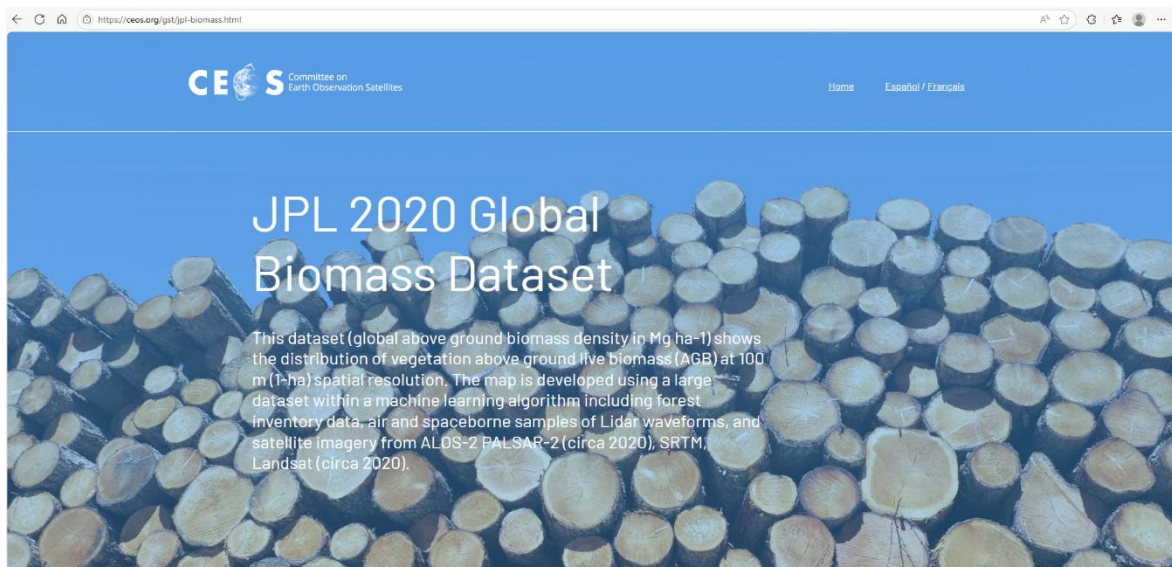
Published by Copernicus Publications.

(Santoro, M.; Cartus, O. (2025): *ESA Biomass Climate Change Initiative (Biomass_cci): Global datasets of forest above-ground biomass for the years 2007, 2010, 2015, 2016, 2017, 2018, 2019, 2020, 2021 and 2022, v6.0. NERC EDS Centre for Environmental Data Analysis, 17 April 2025. doi:10.5285/95913ffb6467447ca72ce9d8cf30501.*)

2. JPL 2020 Global Biomass Dataset <https://ceos.org/gst/jpl-biomass.html>



This dataset displays the distribution of above-ground live biomass (AGB) of vegetation at a 100m (1-hectare) spatial resolution. The map is created using a large dataset combined with machine learning algorithms, including forest inventory data, airborne and spaceborne LiDAR waveform samples, and satellite imagery from ALOS-2, SRTM, and LANDSAT.



1. Three primary strata were defined based on forest type
 - a. Stratum-I: Dry Dipterocarp forest (DDF)
 - b. Stratum-II: Dry Evergreen forest (DEF)
 - c. Stratum-III: Secondary forest (SF)

Each stratum is further divided into sub-strata using AGB data. ArcGIS software is used to calculate biomass statistics via the “**Zonal Statistics as Table**” function.

Zonal Statistics as Table

Input raster or feature zone data
foresttypes2561_sakaerat

Zone field
ftype_code

Input value raster
AGB_Sakarati.tif

Output table
H:\Backup-12July2023\11-อบรมให้กรมป่าไม้ การเก็บคาร์บอนในป่าชุมชน\SKL_Statistics\stat_agb1

☐ Ignore NoData in calculations (optional)

Statistics type (optional)
ALL

OK Cancel Environments... Show Help >>

Table

Stat_AGB

Rowid	FTYPE_CODE	COUNT	AREA	MIN	MAX	RANGE	MEAN	STD	SUM
1	112	126180	0.004319	26.187653	231.676285	205.488632	137.074432	36.120214	17296051.874863
2	122	28530	0.000976	28.208479	138.93544	110.726961	66.135445	13.148347	1886844.243944
3	140	30406	0.001041	24.964046	228.343292	203.379246	118.970564	31.495337	3617418.962416

(0 out of 3 Selected)

Area of stratum-I = $[126,180 \text{ (pixel)} \times 400(\text{m}^2)]/10,000(\text{m}^2) = 5047.2 \text{ ha.}$
 Area of stratum-II = $[28,530 \text{ (pixel)} \times 400(\text{m}^2)]/10,000(\text{m}^2) = 1,141.2 \text{ ha.}$
 Area of stratum-III = $[30,406 \text{ (pixel)} \times 400(\text{m}^2)]/10,000(\text{m}^2) = 1,216.24 \text{ ha.}$

Select by Attributes

Enter a WHERE clause to select records in the table window.

Method : Create a new selection

Attributes:

- "f_code"
- "ftype_code"
- "ftype_thai"
- "ftype_eng"
- "Shape_Leng"

Operator	Value
=	112
< >	122
Like	140
>	
> =	
And	
<	
< =	
Or	
_ %	
()	
Not	
Is	
In	
Null	

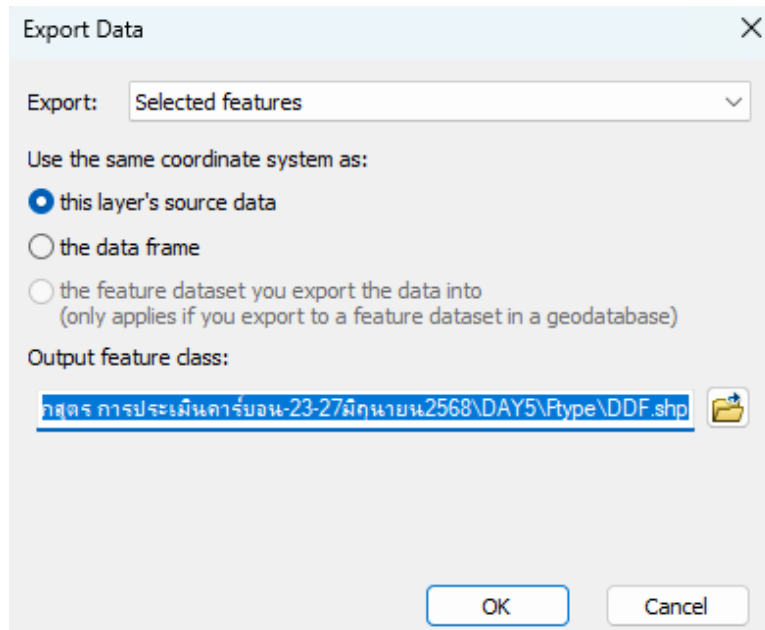
Get Unique Values Go To:

SELECT * FROM foresttypes2561_sakaerat WHERE:
 "ftype_code" = 122

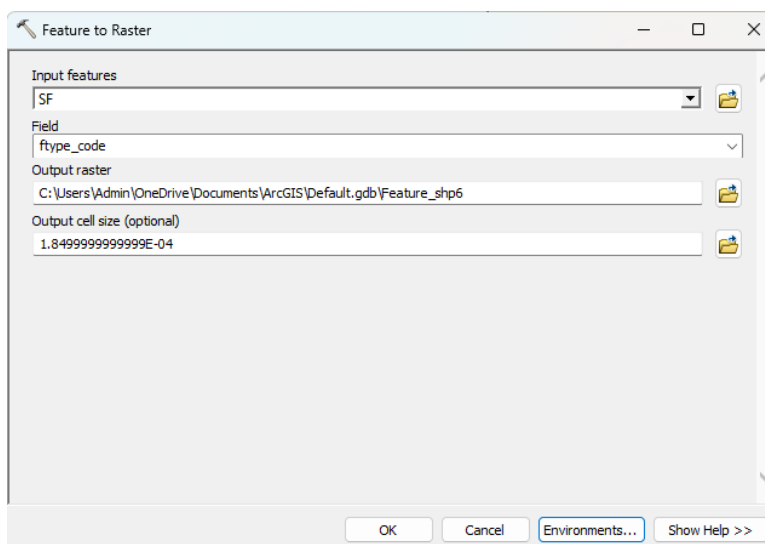
Clear Verify Help Load... Save... Apply Close

2. In the Attribute Table, select the areas separate by forest type using the **Select by Attributes function**, extracting areas by forest type using **ftype_code**.

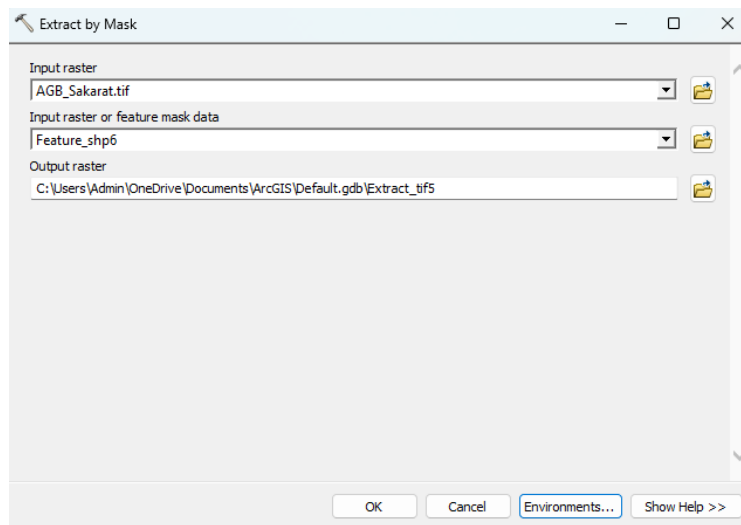
Code	Forest type
112	Dry evergreen forest; DEF
122	Dry dipterocarp forest; DDF
140	Secondary forest; SF



3. Go back to the **Table of Contents** window, and export the selected shapefile according to the forest type, which is in the format of a shapefile.



4. To convert each type of forest shapefile into Raster data, you can choose the function of feature to raster.



5. Extract data based on the AGB density of each type of forest using the **Extract by mask (Spatial Analysis)**.

The result will extract only the boundary of each forest type, allowing the biomass values to be used for sub-stratum classification within the area of interest.

To consider the distribution of AGB within each of type of forest. It can use histogram of AGB, which displays essential values to use the next step such as Mean, Standard deviation (SD), Maximum (Max), and Minimum value (Min).

For example, the statistic of AGB within **Secondary forest** can extract values as followed

Mean = 118.93 t/ha,
Std = 31.50 t/ha,
Min = 24.9 t/ha,

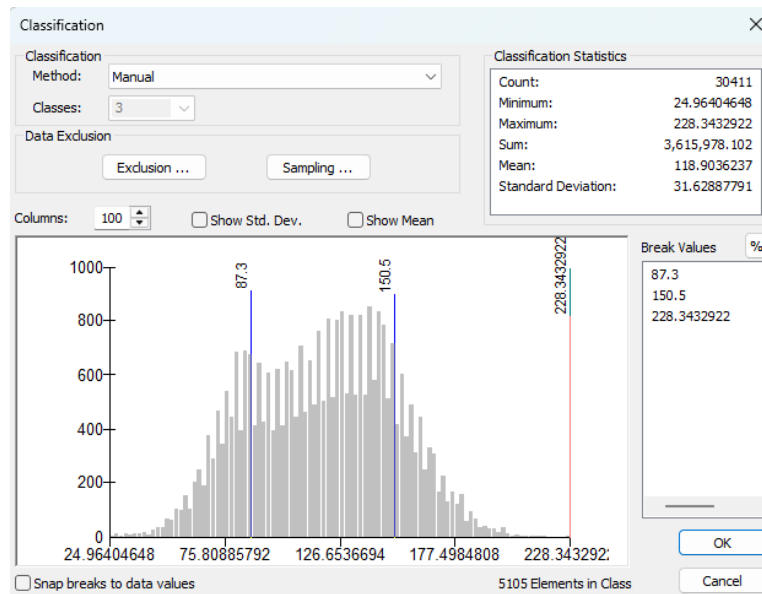
Max = 228.34 t/ha.

Three strata of **Secondary forest (sub-stratum)** were classified by considering the AGB statistics within the forest boundary as follows:

Stratum1 (Min to Mean-SD)

Stratum2 (Mean-SD to Mean+SD)

Stratum3 (Mean+SD to Max)



Reclassify

Input raster: Extract.tif5
 Reclass field: VALUE
 Reclassification:

Old values	New values
24.964046 - 87.3	1
87.3 - 150.5	2
150.5 - 228.343292	3
NoData	NoData

Buttons: Classify..., Unique, Add Entry, Delete Entries, Load..., Save..., Reverse New Values, Precision...

Output raster: C:\Users\Admin\OneDrive\Documents\ArcGIS\Default.gdb\Reclass_Extr2
☐ Change missing values to NoData (optional)

Buttons: OK, Cancel, Environments..., Show Help >>

Zonal Statistics as Table

Input raster or feature zone data: Reclass_Extr2_SecondaryForest
 Zone field: Value
 Input value raster: Extract.tif5
 Output table: C:\Users\Admin\OneDrive\Documents\ArcGIS\Default.gdb\ZonalSt_Reclass2
☒ Ignore NoData in calculations (optional)
 Statistics type (optional): ALL

Buttons: OK, Cancel, Environments..., Show t

Table

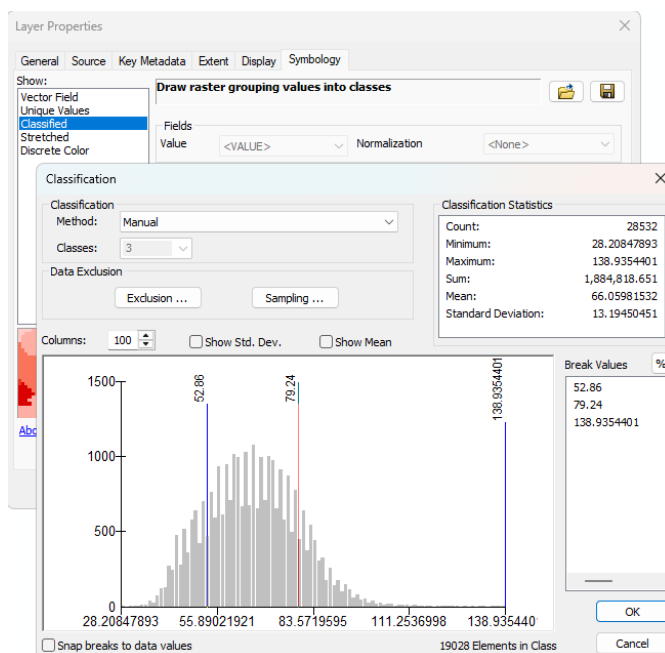
ZonalSt_Reclass2

OBJECTID	Value	COUNT	AREA	MIN	MAX	RANGE	MEAN	STD	SUM
1	1	5931	0.000203	24.964046	87.293915	62.329868	73.937192	10.486901	438521.486601
2	2	19378	0.000663	87.301826	150.49942	63.197594	120.745731	18.006964	2339810.773216
3	3	5102	0.000175	150.500153	228.343292	77.84314	164.35884	11.23715	838558.799271

Reclassify data in **Secondary forest**, which used the definition from a previous step.

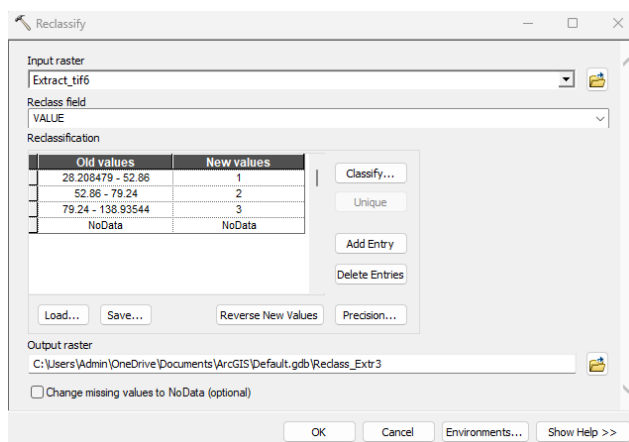
6. To summarize values of a raster within the zones of another dataset (**substratum**) and report the statistical result by using Zonal statistics as a **Table (Spatial Analyst)**.

The analysis in the **Dry Dipterocarp Forest (DDF)** and **Dry Evergreen Forest (DEF)** areas was conducted according to steps 4-6, with biomass statistics for each forest type recorded to enable the calculation of the optimal number of sample plots using the Winrock tool.



A G B of **Dry dipterocarp forest** boundary can extract the statistics values as follows

Mean = 66.12 t/ha
Std = 13.14 t/ha
Min = 28.20 t/ha
Max = 138.93 t/ha

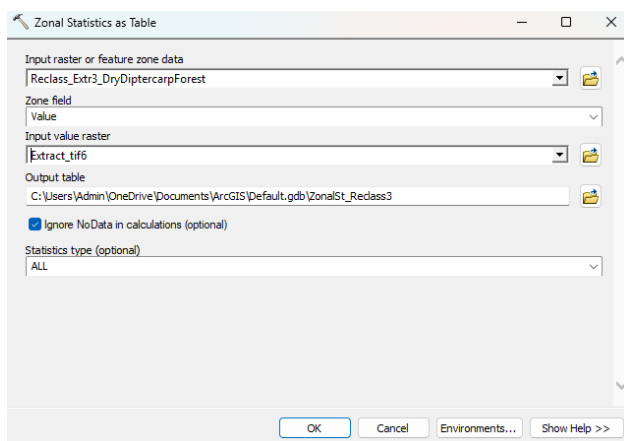


Three strata of **Dry dipterocarp forest (sub-stratum)** were classified by considering AGB statistics within the forest boundary as follows:

Stratum1 (Min to Mean-SD)

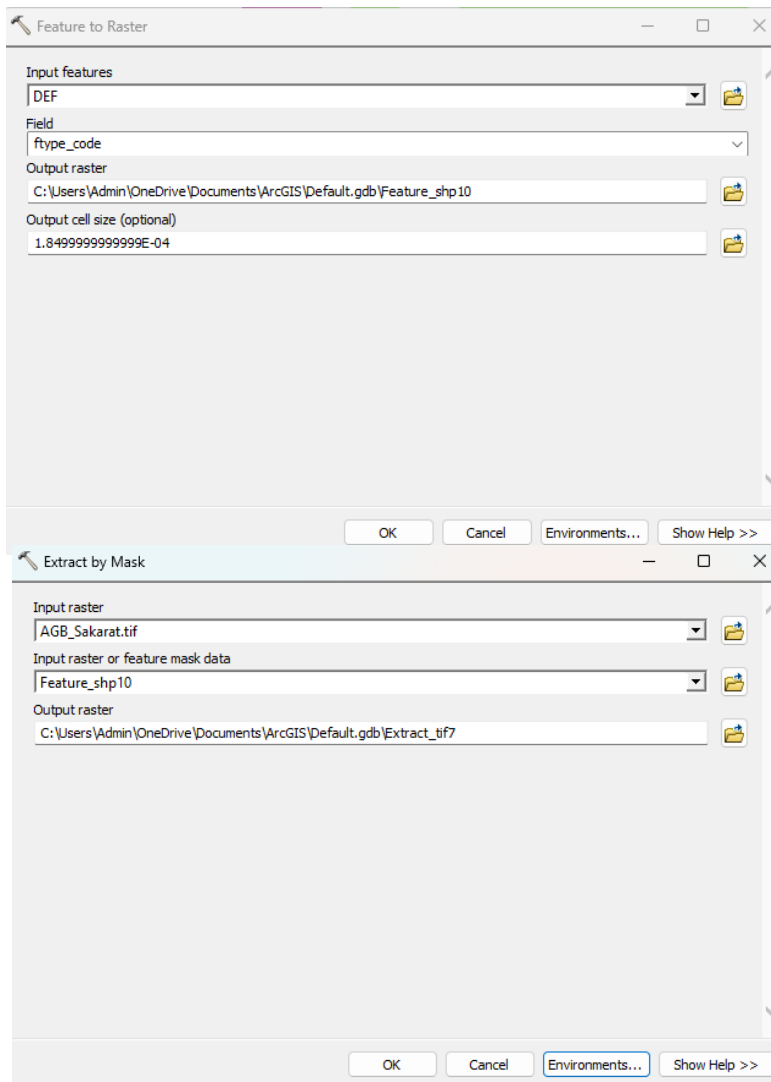
Stratum2 (Mean-SD to Mean+SD)

Stratum3 (Mean+SD to Max)



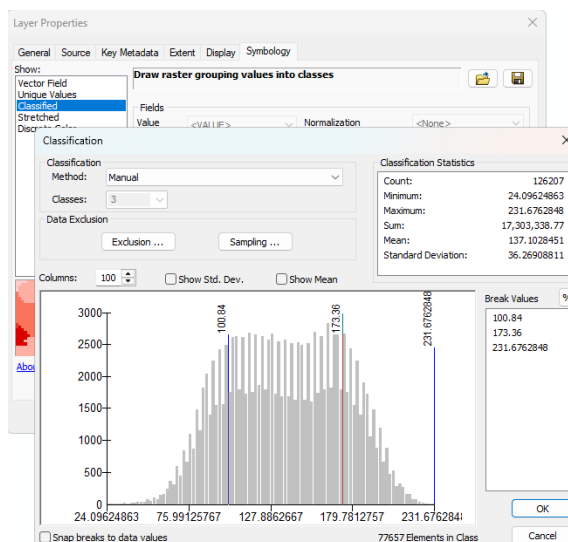
To summarize values of a raster within the zones of another dataset (**substratum**) and report the statistical result by using Zonal statistics as a **Table** (Spatial Analyst).

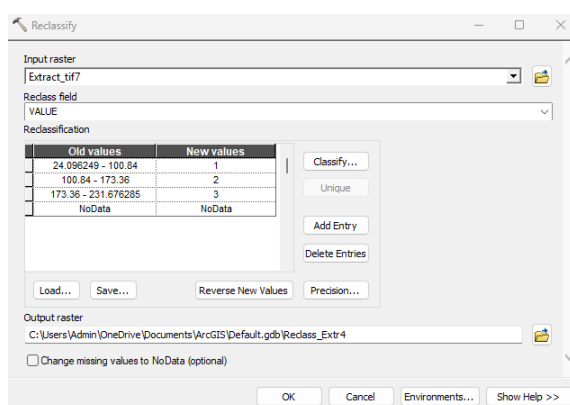
ZonalSt_Reclass3_DryDipterocarpForest									
Value	COUNT	AREA	OBJECTID *	MIN	MAX	RANGE	MEAN	STD	SUM
1	4878	0.000167	1	28.208479	52.858536	24.650057	47.292839	3.865738	230694.470846
2	19025	0.000651	2	52.865738	79.23938	26.373642	66.028918	7.260265	1256200.16268
3	4629	0.000158	3	79.242935	138.93544	59.692505	86.382475	6.932847	399864.477493



AGB of **Dry Evergreen forest** can extract values as follows

Mean = 137.06 t/ha
 Std = 36.12 t/ha
 Min = 24.09 t/ha
 Max = 231.67 t/ha



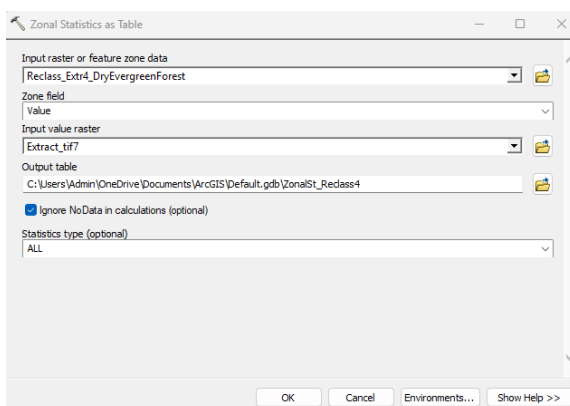


Three strata of **Dry evergreen forest (sub-stratum)** were classified by considering the AGB statistics within the forest boundary as follows:

Stratum1 (Min to Mean-SD)

Stratum2 (Mean-SD to Mean+SD)

Stratum3 (Mean+SD to Max)



To summarize values of a raster within the zones of another dataset (**sub-stratum**) and reports the statistic result by using **Zonal statistics as Table (Spatial Analyst)**.

OBJECTID	Value	COUNT	AREA	MIN	MAX	RANGE	MEAN	STD	SUM
1	1	24095	0.000	24.0962	100.838	76.742	86.0307	11.180	2072911.877
2	2	78000	0.002	100.840	173.359	72.518	137.216	21.118	10702918.04
3	3	24112	0.000	173.360	231.676	58.315	187.582	10.451	4522996.821

Table1. Summarization of AGB Statistics each of sub-stratums categorized by forest type.

Type of forest/sub-stratum	Area (ha.)	Mean	Std
Secondary forest	237.24	73.93	10.48

	Sub-stratum2	775.12	120.74	18.00
	Sub-stratum3	204.08	164.35	11.23
Dry dipterocarp	Sub-stratum4	162.80	47.29	3.86
	Sub-stratum5	761.00	66.02	7.26
	Sub-stratum6	185.16	86.38	6.93
Dry evergreen	Sub-stratum7	963.80	86.03	11.18
	Sub-stratum8	3,120.00	137.21	21.11
	Sub-stratum9	964.48	187.58	10.45

Calculation of the number of sample plots for measurements within A/R CDM Project activities

Winrock International's CDM A/R sample plot calculator spreadsheet_tool.

(<https://globalclimateactionpartnership.org/resource/winrock-internationals-cdm-ar-sample-plot-calculator-spreadsheet-tool/>)

Methodology

1. Stratified Random Sampling: The study area was divided into strata based on variables such as forest type. Random plots were selected within each stratum to ensure representative coverage.

2. Sample Size Estimation: Plot numbers were determined from the standard deviation of biomass within strata, desired confidence levels (90%–95%), and an acceptable error margin ($\pm 10\%$).

3. Cost Optimization: Sampling design balanced statistical requirements with field costs, plot accessibility, and time constraints.

4. Normal Distribution Assumption: The approach assumes normally distributed carbon accumulation, though heterogeneous landscapes may cause deviations.

5. Permanent Plot Design: Permanent plots were established for long-term monitoring, improving precision, and capturing temporal trends.

Open the Winrock International CDM A/R Sample Plot Calculator (Excel) and enter the statistical values calculated from Table 1 into the **Biomass Stocks-Plots** worksheet, using hectares as the unit of measurement.

Step 1. To indicate the Level of error and Confidence error

STEP 1 Input level of acceptable error and confidence level		
REQUIRED ERROR AND CONFIDENCE LEVEL		
Level of error (%)	10.0%	from CDM tool: "A default value of 10% may be used unless a different value is prescribed in a methodology"
Confidence level	90%	Allowable entries: 80%, 90%, 95%, 98%, 99% from CDM tool: "Use the 90% confidence level for determination of biomass stock in A/R CDM project activities, unless a different confidence level is prescribed in a methodology"

Step2. Input Stratum information

STEP 2 Input Stratum information									
Sampling Characteristics of each stratum									
Stratum	Stratum Name	Area (ha)	Mean Biomass (t dry matter ha ⁻¹)	Standard Deviation (t dry matter ha ⁻¹)	Plot size (ha)	Intermediate Calculations			
						N _i	w _i	w _i * s _i	w _i * s _i ²
stratum 1	sub-stratum1	237.24	73.93	10.48	0.16	1,482.75	0.03	0.34	3.53
stratum 2	sub-stratum2	775.12	120.74	18	0.16	4,844.50	0.11	1.89	34.06
stratum 3	sub-stratum3	204.08	164.35	11.23	0.16	1,275.50	0.03	0.31	3.49
stratum 4	sub-stratum4	162.8	47.29	3.86	0.16	1,017.50	0.02	0.09	0.33
stratum 5	sub-stratum5	761	66.02	7.26	0.16	4,756.25	0.10	0.75	5.44
stratum 6	sub-stratum6	185.16	86.38	6.93	0.16	1,157.25	0.03	0.17	1.21
stratum 7	sub-stratum7	963.8	86.03	11.18	0.16	6,023.75	0.13	1.46	16.34
stratum 8	sub-stratum8	3120	137.21	21.11	0.16	19,500.00	0.42	8.93	188.56
stratum 9	sub-stratum9	964.48	187.58	10.45	0.16	6,028.00	0.13	1.37	14.28
stratum 10									
stratum 11									
stratum 12									
stratum 13									
stratum 14									
stratum 15									
stratum 16									
stratum 17									
stratum 18									
stratum 19									
stratum 20									

Enter the statistical values for each sub-stratum, calculated using forest type data and AGB accumulation data for that sub-stratum (expressed in hectares). Once the data have been entered, the computation will be performed automatically using Equation 1.

Equation 1

$$n = \frac{N * t_{VAL}^2 (\sum_i w_i * s_i)^2}{N * E^2 + t_{VAL}^2 * \sum_i w_i * s_i^2}$$

Step3. Calculate the intermediate results.

To conduct a preliminary assessment of whether the calculated value of n is greater than or equal to 30, where n represents the total number of plots required to achieve the specified level of precision for the project area.

If n is less than 30, the calculation will be repeated using Equation 1, with the degrees of freedom set to $n - 1$ and the t -value obtained from the Student's t -distribution table. The resulting value will be displayed in Cell P21.

STEP 3 Intermediate Results								
Calculations completed automatically								
Stratum	Stratum Name	Intermediate Calculations				Equation 3		Equation 2
		Equation 1	Equation 1		Sampling faction (large = area sampled >5% of project area, small = area sampled <5% of project area)	Use only if have Large Sampling Fraction (>5%)	O R	Use only if have Small Sampling Fraction (<5%)
		Plot Quantity (n) First Iteration	Plot Quantity (n) Second Iteration (if n<30)	Sampling Area (ha)	Plot quantity (n) adjusted for large sampling fraction	(n) simplified for small sampling fraction		
Total Sample Size		4	8.51	1.36	0.018%	9		4
stratum 1	sub-stratum1		0.19	0.03		0.2		0.1
stratum 2	sub-stratum2		1.05	0.17		1.1		0.5
stratum 3	sub-stratum3		0.17	0.03		0.2		0.1
stratum 4	sub-stratum4		0.05	0.01		0.0		0.0
stratum 5	sub-stratum5		0.42	0.07		0.4		0.2
stratum 6	sub-stratum6		0.10	0.02		0.1		0.0
stratum 7	sub-stratum7		0.81	0.13		0.8		0.4
stratum 8	sub-stratum8		4.96	0.79		5.0		2.4
stratum 9	sub-stratum9		0.76	0.12		0.8		0.4
stratum 10								
stratum 11								
stratum 12								
stratum 13								
stratum 14								
stratum 15								
stratum 16								
stratum 17								
stratum 18								
stratum 19								
stratum 20								

Equation 2

$$n = \left(\frac{t_{VAL}}{E} \right)^2 * \left(\sum_i w_i * s_i \right)^2$$

Equation 3

$$n_a = n * \frac{1}{1 + n/N}$$

Step 4. Results.

For the CDM A/R Tool, if the sampling area is large—defined as exceeding 5% of the total study area—the number of sample plots obtained from Equation 1 shall be adjusted using Equation 3, with the result displayed in **Cell S21**. Conversely, if the sampling area is small—less than 5% of the study area—the calculation shall be performed using Equation 2, and the result will be displayed in **Cell U21**.

Finally, the number of plots to be randomly selected within each sub-stratum shall be calculated using Equation 4.

STEP 4 - Results		
Total number of plots and number of plots per stratum. Calculated using correct equation, based on 'sampling fraction'. Results rounded into an integer		
Stratum Stratum Name		Calculated sampling fraction size:
		Small fraction (Equation 2 used)
		Plot quantity (n) simplified for small sampling fraction
Total Sample Size		4
stratum 1	sub-stratum1	0
stratum 2	sub-stratum2	1
stratum 3	sub-stratum3	0
stratum 4	sub-stratum4	0
stratum 5	sub-stratum5	0
stratum 6	sub-stratum6	0
stratum 7	sub-stratum7	0
stratum 8	sub-stratum8	2
stratum 9	sub-stratum9	0
stratum 10		
stratum 11		
stratum 12		
stratum 13		
stratum 14		
stratum 15		
stratum 16		
stratum 17		
stratum 18		
stratum 19		
stratum 20		

Equation 4	$n_i = n * \frac{w_i * S_i}{\sum_i w_i * S_i}$
------------	--

Step 5. Final estimate of plots

STEP 5 - Final estimate of plots

NOTE: This step is NOT included in the CDM A/R Methodological tool

The CDM tool presents the required number of plots based on specific targeted precision. However, it is advisable additional plots be installed as a precaution. Actual conditions may vary from those found in preliminary data.

Percent additional plots:

10%

It is recommended that at least 10-20% more plots be installed than CDM tool equations calculate

Stratum	Stratum Name	Final plot quantity (n)
Total Sample Size		4
stratum 1	sub-stratum1	0
stratum 2	sub-stratum2	1
stratum 3	sub-stratum3	0
stratum 4	sub-stratum4	0
stratum 5	sub-stratum5	0
stratum 6	sub-stratum6	0
stratum 7	sub-stratum7	0
stratum 8	sub-stratum8	2
stratum 9	sub-stratum9	0
stratum 10		
stratum 11		
stratum 12		
stratum 13		
stratum 14		
stratum 15		
stratum 16		
stratum 17		
stratum 18		
stratum 19		
stratum 20		

Reference

- Avitabile, V., Herold, M., Heuvelink, G., Lewis, S.L., Phillip, O.L., Asner, G.P., Armston, J., Ashton, P.S., Banin, L. and Bayol, N., 2016. An integrated pan-tropical biomass map using multiple reference datasets. *Global Change Biology*, pp. 1406-1420.
- Baccini, A., Goetz, S.J., Walker, W.S., Laporte, N.T., Sun, M., Sulla-Menashe, D., Hackler, J., Beck, P., Dubayah, R. and Friedl, M.A., 2012. Estimated carbon dioxide emissions from tropical deforestation improved by carbon-density maps. *Nature climate change*, pp. 182-185.
- Balzter, H., 2001. Forest mapping and monitoring with interferometric synthetic aperture radar (InSAR). *Progress in physical geography*, 25(2), pp. 159-177.
- Banda, F., Giudici, D., Le Toan, T., Alessandro, M.M., Papathanassiou, K., Quegan, S., Riembauer, G., Scipal, K., Soja, M., Tebaldini, S., Ulander, L. and Villard, L., 2020. The BIOMASS level2 prototype preprocessor: design and experimental results of above-ground biomass estimation. *Remote sensing*, 12(6), p. 985.
- Barbosa, J.M., Broadbent, E.N. and Bitencourt, M.D., 2014. Remote sensing of aboveground biomass in tropical secondary forests: a review. *International Journal of Forestry Research*, pp. 1-14.
- Bonan GB. Forests and climate change: forcings, feedbacks, and the climate benefits of forests. *Science*. 2008;320(5882):1444–9. doi:10.1126/science.1155121.
- Brys, R., Jacquemyn, H. and De Blust, G., 2005. Fire increases aboveground biomass, seed production and recruitment success of *Molinia caerulea* in dry heathland. *Acta Oecologica*, 28(3), pp. 299-305.
- Chave, J., Coomes, D., Jansen, S., Lewis, S.L., Swenson, N.G. and Zanne, A.E., 2009. Towards a worldwide wood economics spectrum. *Ecology letters*, 12(4), pp. 351-366.
- Despotovic, M., Nedic, V., Despotovic, D. and Cvetanovic, S., 2016. Evaluation of empirical models for predicting monthly mean horizontal diffuse solar radiation. *Renewable and Sustainable Energy Reviews*, 56, pp.246-260.
- Dobson, M.C., Ulaby, F.T., LeToan, T., Beaudoin, A., Kasischke, E.S. and Christensen, N., 1992. Dependence of radar backscatter on coniferous forest biomass. *IEEE Transactions on Geoscience and remote sensing*, 30(2), pp. 412-415.
- Eggleston, H.S., Buendia, L., Miwa, K., Ngara, T. and Tanabe, K., 2006. *2006 IPCC Guidelines for National Greenhouse Gas Inventories, Prepared by the National Greenhouse Gas Inventories Programme*, Japan: IGES.
- Englhart, S., Keuck, V. and Siegert, F., 2011. Modeling aboveground biomass in tropical forests using multi-frequency SAR data-A comparison of methods. *IEEE Journal of Selected Topics in Applied Earth Observations and Remote Sensing*, 5(1), pp. 298-306.
- Foody, G.M., Boyd, D.S. and Cutler, M.E., 2003. Predictive relations of tropical forest biomass from Landsat TM data and their transferability between regions. *Remote Sensing of Environment*, 85(4), pp. 463-474.
- Franklin, J., 2010. *Mapping species distribution: spatial inference and prediction (Ecology, Biodiversity and Conservation)*. Cambridge, UK.: Cambridge University Press.
- Fransson, J.E.S., 1999. Estimation of stem volume in boreal forests using ERS-1 C- and JERS-1 L-band SAR data. *International Journal of Remote Sensing*, 20(1), pp. 123-137.
- Gaveau, D.L., Balzter, H. and Plummer, S., 2003. Forest woody biomass classification with satellite-based radar coherence over 900 000 km² in Central Siberia. *Forest Ecology and Management*, 174(1-3), pp. 65-75.



- Ghatak, A., 2017. *Machine learning with R*. Singapore: Springer.
- Gibbs, H.K., Brown, S., Niles, J.O. and Foley, J.A., 2007. Monitoring and estimating tropical forest carbon stocks: making REDD a reality. *Environmental research letters*, 2(4), p. 045023.
- GOFC-GOLD, 2016. *A sourcebook of methods and procedures for monitoring and reporting anthropogenic greenhouse gas emissions and removals associated with deforestation, gains and losses of carbon stocks in forests remaining forests, and forestation*, Wageningen, The Netherlands: GOFC-GOLD Land Cover Project Office.
- Gonzalez, P., Kroll, B. and Vargas, C.R., 2014. Tropical rainforest biodiversity and aboveground carbon changes and uncertainties in the selva central, Peru. *Forest Ecology and Management*, Volume 312, pp. 78-91.
- Hackeling, G., 2014. *Mastering Machine Learning with scikit-learn*. 2nd ed. Birmingham, UK.: Packt Publishing Ltd..
- Heinänen, S., Erola, J. and Von Numers, M., 2012. High resolution species distribution models of two nesting water bird species: a study of transferability and predictive performance. *Landscape Ecology*, 27(4), pp. 545-555.
- Houghton, R. A., 2005. Aboveground forest biomass and the global carbon balance. *Global Change Biology*, Volume 11, pp. 945-958.
- Houghton, R.A., Hall, F. and Goetz, S.J., 2009. Importance of biomass in the global carbon cycle. *Journal of Geophysical Research*, Volume 114, pp. 1-13.
- Hu, T., Su, Y., Xue, B., Liu, J., Zhao, X., Fang, J. and Guo, Q., 2016. Mapping global forest aboveground biomass with spaceborne LiDAR, optical imagery, and forest inventory data. *Remote Sensing*, Volume 8, pp. 1-27.
- Hubbard, W., Biles, L., Mayfield, C. and Ashton, S., 2007. *Sustainable forestry for bioenergy and bio-based products: Trainers curriculum notebook*. Athens, GA: Southern forest research partnership Inc..
- Imhoff, M.L., 1995b. Radar backscatter and biomass saturation: Ramifications for global biomass inventory. *IEEE Transactions on Geoscience and Remote Sensing*, 33(2), pp. 511-518.
- IPCC. Climate Change: Synthesis Report 2014. Contribution of Working Groups I, II and III to the Fifth Assessment Report of the Intergovernmental Panel on Climate Change [Core writing team R.K. Pachauri and L.A. Meyer (eds.)]. Geneva, Switzerland: IPCC2014 2014. Report No.: 9291691437.
- Koch, B., 2010. Status and future of laser scanning, synthetic aperture radar and hyperspectral remote sensing data for forest biomass assessment. *ISPRS Journal of Photogrammetry and Remote sensing*, 65(6), pp.581-590.
- Le Toan, T., Picard, G., Martinez, J. M., Melon, P. and Davidson, M., 2002. *On the relationships between radar measurements and forest structure and biomass*. Sheffield, UK., in Retrieval of Bio-and Geo-Physical Parameters from SAR Data for Land Applications European Space Agency, pp. 3-12.
- Liang, S. and Wang, J., 2019. *Advanced remote sensing: terrestrial information extraction and applications*.. 2nd ed. London, UK.: Academic Press is an imprint of Elsevier.
- Lu, D., 2006. The potential and challenge of remote sensing-based biomass estimation. *International journal of remote sensing*, 27(7), pp. 1297-1328.
- Lu, D., Chen, Q., Wang, G., Liu, L., Li, G. and Moran, E., 2016. A survey of remote sensing-based aboveground biomass estimation methods in forest ecosystems. *International Journal of Digital Earth*, 9(1), pp. 63-105.

- Lucas, R., Armston, J., Fairfax, R., Fensham, R., Accad, A., Carreiras, J., Kelley, J., Bunting, P., Clewley, D., Bray, S. and Metcalfe, D., 2010. An evaluation of the ALOS PALSAR L-band backscatter—Above ground biomass relationship Queensland, Australia: Impacts of surface moisture condition and vegetation structure. *IEEE Journal of Selected Topics in Applied Earth Observations and Remote Sensing*, 3(4), pp. 576-593.
- Luckman, A., Baker, J., Kuplich, T.M., Yanasse, C.D.C.F. and Frery, A.C., 1997. A study of the relationship between radar backscatter and regenerating tropical forest biomass for spaceborne SAR instruments. *Remote Sensing of Environment*, 60(1), pp. 1-13.
- Mohri, M., Rostamizadeh, A. and Talwalkar, A., 2018. *Foundations of Machine Learning*. 2nd ed. Massachusetts, US: The MIT Press.
- Michard, E.T., Saatchi, S.S., Woodhouse, I.H., Nangendo, G., Ribeiro, N.S., Williams, M., Ryan, C.M., Lewis, S.L., Feldpausch, T.R. and Meir, P., 2009. Using satellite radar backscatter to predict above-ground woody biomass: A consistent relationship across four different African landscapes. *Geophysical Research Letters*, 36(23).
- Minh, D., Ndikumana, E., Vieilledent, G., McKey, D. and Baghdadi, N., 2018. Potential value of combining ALOS PALSAR and Landsat-derived tree cover data for forest biomass retrieval in Madagascar. *Remote Sensing of Environment*, Volume 213, pp. 206-214.
- Næsset, E., 2007. Airborne laser scanning as a method in operational forest inventory: Status of accuracy assessments accomplished in Scandinavia. *Scandinavian Journal of Forest Research*, 22(5), pp. 433-442.
- Ningthoujam, R.K., Balzter, H., Tansey, K., Morrison, K., Johnson, S., Gerard, F., Malhi, Y., Burbidge, G., Doody, S. and Veck, N., 2016. Airborne S-band SAR for forest biophysical retrieval in temperate mixed forests of the UK. *Remote Sensing*, 8(7), p. 609.
- Peregon, A. and Yamagata, Y., 2013. The use of ALOS/PALSAR backscatter to estimate above-ground forest biomass: A case study in Western Siberia. *Remote Sensing of Environment*, Volume 137, pp. 139-146.
- Pizaña, J.M.G., Hernández, J.M.N. and Romero, N., 2016. Remote sensing-based biomass estimation. *Environmental Application of Remote Sensing*, Volume 1.
- Quegan, S., Rauste, Y., Bouvet, A., Carreiras, J., Cartus, O., Carvalhals, N., LeToan, T., Mermoz, S. and Santoro, M., 2017. *D6-Global Biomass Map Algorithm Theoretical Basis Document*. [Online] Available at: https://GlobBiomass.org/wpcontent/uploads/DOC/Deliverables/D6_D7/GlobBiomass_D6_7_Global_ATBD_v2.pdf [Accessed 3 September 2020].
- Ranson, K.J., Sun, G., Weishampel, J.F. and Knox, R.G., 1997. Forest biomass from combined ecosystem and radar backscatter modeling. *Remote Sensing of Environment*, 59(1), pp. 118-133.
- Rocchini, D., Foody, G.M., Nagendra, H., Ricotta, C., Anand, M., He, K.S., Amici, V., Kleinschmit, B., Frster, M. and Schmidlein, S., 2013. Uncertainty in ecosystem mapping by remote sensing. *Computers and Geosciences*, Volume 50, pp. 128-135.
- Rodriguez-Veiga, P., Saatchi, S., Tansey, K. and Balzter, H., 2016. Magnitude, spatial distribution and uncertainty of forest biomass stocks in Mexico. *Remote Sensing of Environment*, Volume 183, pp. 265-281.
- Rodriguez-Veiga, P., Wheeler, J., Louis, V., Tansey, K. and Balzter, H., 2017. Quantifying forest biomass carbon stocks from space. *Current Forestry Reports*, 3(1), pp. 1-18.



- Saatchi, S.S., Harris, N.L., Brown, S., Lefsky, M., Mitchard, E.T., Salas, W., Zutta, B.R., Buermann, W., Lewis, S.L., Hagen, S., Petrova, S., White, L., Silman, M., Morel, A., 2011. Benchmark map of forest carbon stocks in tropical regions across three continents. *Proceeding of the National Academy of Sciences*, Volume 108, pp. 9899-9904.
- Saatchi, S.S. Houghton, R.A., Dos Santos Alvala, R.C., Soares, J.V. and Yu, Y., 2007. Distribution of aboveground live biomass in the Amazon basin. *Global change biology*, 13(4), pp. 816-837.
- Santoro, M., Askne, J. and Dammert, P., 2005. Tree height influence on ERS interferometric phase in boreal forest. *IEEE Transactions on Geoscience and Remote Sensing*, 43(2), pp. 207-217.
- Santoro, M. and Cartus, O., 2018. Research pathways of forest above-ground biomass estimation based on SAR backscatter and interferometric SAR observations. *Remote Sensing*, 10(4), p. 608.
- Santoro, M., Cartus, O., Mermoz, S., Bouvet, A., Le Toan, T., Carvalhais, N., Rozendaal, D., Herold, M., Avitabile, V., Quegan, S. and Carreiras, J., 2018a. A detailed portrait of the forest aboveground biomass pool for the year 2010 obtained from multiple remote sensing observations. *EGUGA*, p. 18932.
- Santoro, M., Cartus, O., Schmullius, C., Wegmüller, U., Werner, C., Wiesmann, A., Pang, Y. and Li, Z., 2006. On the generation of a forest biomass map for Northeast China: SAR interferometric processing and development of classification algorithm. *In Fringe 2005 Workshop*, Volume 610.
- Santoro, M., Wegmüller, U. and Askne, J., 2018b. Forest stem volume estimation using C-band interferometric SAR coherence data of the ERS-1 mission 3-days repeat-interval phase. *Remote Sensing of Environment*, Volume 216, pp. 684-696.
- Santos, J.R., Freitas, C.C., Araujo, L.S., Dutra, L.V., Mura, J.C., Gama, F.F. and Luciana, S., 2003. Airborne P-band SAR applied to the aboveground biomass studies in the Brazilian tropical rainforest. *Remote Sensing of Environment*, 87(4), pp. 482-493.
- Sinha, S., Jeganathan, C., Sharma, L.K. and Nathaw, M.S., 2015. A review of radar remote sensing for biomass estimation. *International Journal of Environmental Science and Technology*, 12(5), pp. 1779-1792.
- Song, C., 2013. Optical remote sensing of forest leaf area index and biomass. *Progress in Physical Geography*, 37(1), pp.98-113.
- Su, Y., Guo, Q., Xue, B., Hu, T., Alvarez, O., Tao, S. and Fang, J., 2016. Spatial distribution of forest aboveground biomass in China: Estimation through combination of spaceborne lidar, optical imagery, and forest inventory data. *Remote Sensing of Environment*, Volume 173, pp. 187-199.
- Sun, G., Ranson, K.J., Guo, Z., Zhang, Z., Montesano, P. and Kimes, D., 2011. Forest biomass mapping from lidar and radar synergies. *Remote Sensing of Environment*, 115(11), pp. 2906-2916.
- Wagner, W., Luckman, A., Vietmeier, J., Tansey, K., Balzter, H., Schmullius, C., Davidon, M., Gaveau, D., Gluck, M., Le Toan, T., Quegan, S., Shvidenko, A. and Wiesmann, J.J.Y., 2003. Large-scale mapping of boreal forest in SIBERIA using ERS tandem coherence and JERS backscatter data. *Remote Sensing of Environment*, 85(2), pp. 125-144.
- Wanthongchai, K., 2008. *Effects of difference burning frequencies of fire behavior, nutrient dynamics, soil properties, and vegetation structure and composition in dry dipterocarp forest, Huay Kha Khaeng wildlife Sanctuary, Thailand*. The University of Freiburg, Freiburg: In, Ph.D. diss. Institute of Silviculture, p. 190.

West, P. W., 2009. *Tree and forest measurement*. Berlin, Heidelberg: Springer-Verlag Berlin Heidelberg.

